

**The albite fusion curve re-examined: new experiments and
the density and compressibility of $\text{NaAlSi}_3\text{O}_8$ liquid with pressure**

Travis J. Tenner
Department of Geological Sciences
University of Michigan
1100 N. University Ave.
Ann Arbor, MI 48109-1005






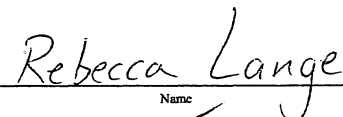
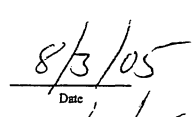
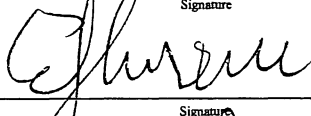
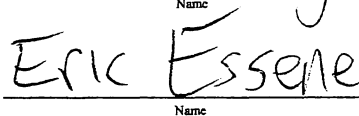
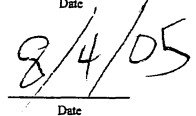
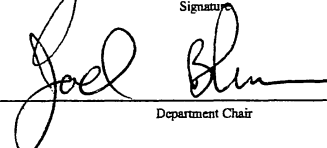
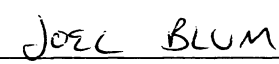
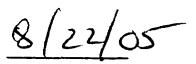
Author
Travis Tenner

Title

The albite fusion curve re-examined: new experiments and the density and compressibility of NaAlSi₃O₈ liquid with pressure


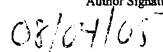
submitted in partial fulfillment
of the requirements for the degree of
Master of Science in Geology
Department of Geological Sciences
The University of Michigan

Accepted by:

 Signature	 Name	 Date
 Signature	 Name	 Date
 Department Chair	 Name	 Date

I hereby grant the University of Michigan, its heirs and assigns, the non-exclusive right to reproduce and distribute single copies of my thesis, in whole or in part, in any format. I represent and warrant to the University of Michigan that the thesis is an original work, does not infringe or violate any rights of others, and that I make these grants as the sole owner of the rights to my thesis. I understand that I will not receive royalties for any reproduction of this thesis.

- Permission granted.
- Permission granted to copy after: _____
Date
- Permission declined.


Author Signature


ABSTRACT

A half-reversal on the melting temperature of high albite ($\text{NaAlSi}_3\text{O}_8$) was determined at 2.28 GPa (1360-1370°C) and 2.73 GPa (1383-1389°C) in a piston-cylinder apparatus with $\text{NaAlSi}_3\text{O}_8$ glass as the starting material. A detailed thermal gradient across the sample capsule was mapped, which showed a 3.5 °C gradient across the upper third of the sample capsule and a 30 °C gradient across the lower two-thirds. A calibration against the melting curve of NaCl showed a -9 % pressure correction for the $\text{BaCO}_3/\text{MgO}/\text{graphite}$ pressure medium used in these experiments. In addition to the glass-crystal half-reversal, a crystal-glass half-reversal at 2.73 GPa was obtained (1389-1399°C) using high albite as the starting material. All run products that quenched to a glass were analyzed by Fourier-transform infrared spectroscopy and found to contain < 0.045 wt % H_2O . The experiments constraints on albite fusion are in excellent agreement with those of Birch and LeComte (1960) and Boyd and England (1963), but deviate from those of Boettcher et al. (1982). The new data on the albite fusion curve at high pressure are compared with the calculated melting reaction based on the best available thermodynamic data at one bar (Lange, 2003) and various values for the pressure dependence of liquid compressibility ($K'_0 = dK_{T,0}/dP$, where $K_{T,0} = 1/\beta_{T,0}$) for $\text{NaAlSi}_3\text{O}_8$ liquid, using the 3rd-order Birch-Murnaghan equation of state. The phase-equilibrium data match the fusion curve calculated with a liquid K'_0 value of 10.7 ± 0.5 . This allows the density of $\text{NaAlSi}_3\text{O}_8$ liquid to be calculated at 1500°C and 3.0 GPa ($2.546 \pm 0.004 \text{ g/cm}^3$), with an uncertainty that is < 0.2 %. The results of this study show that the density and compressibility of this viscous and fully polymerized liquid can be calculated to high pressure (~3 GPa) with a remarkably high precision. Owing to the

absence of any coordination change in NaAlSi₃O₈ liquid in the range up to ~8 GPa, calculations of its density and compressibility can likely be extended to this pressure.

INTRODUCTION

The congruent melting curves of end-member rock-forming minerals are an essential source of thermodynamic data, especially for their liquid state. Typically the one-bar thermodynamic properties of the crystal and liquid are well known, which allows the pressure dependence of the liquid compressibility ($K'_0 = dK_{T,0} / dP$), where $K_{T,0} = 1/\beta_{T,0}$) to be derived. An experimental determination of the melting reaction in P-T space evaluates the internal consistency of thermodynamic data sets. This study focuses on the equilibria between crystalline disordered (high) albite (NaAlSi₃O₈) and liquid of the same composition.

The equation used to calculate the albite melting curve at temperature and pressure is:

$$\Delta H_{T_f} + \int_{T_f}^T \Delta C_p(T) dT - T \left(\Delta S_{T_f} + \int_{T_f}^T \frac{\Delta C_p(T)}{T} dT \right) = - \int_1^P \Delta V_T(P) dP \quad (1)$$

where T_f is the one-bar melting temperature of crystalline albite, ΔH_{T_f} is the enthalpy of the liquid minus that of the solid at T_f , ΔS_{T_f} is the entropy of the liquid minus that of the solid at T_f , $\Delta C_p(T)$ is the heat capacity of the liquid minus that of the solid, and $\Delta V_T(P)$ is the volume of the liquid minus that of the solid. Among the thermodynamic data required, the only unknown is the pressure dependence of the liquid compressibility, K'_0 , which is needed to calculate the albite fusion curve above 1 GPa (Lange, 2003). The

melting of albite is limited to pressures ≤ 3.3 GPa by the albite = jadeite + quartz reaction (Holland, 1980).

To determine the K'_0 of $\text{NaAlSi}_3\text{O}_8$ liquid, the third-order Birch-Murnaghan equation of state (Birch, 1978) is used, which models the volume of silicate liquids to high pressure (tens of GPa) remarkably well (e.g. Stixrude and Bukowinski, 1990). The third-order form is:

$$P = \frac{3}{2}K_{T,0}(R^{7/3} - R^{5/3}) \left[1 - \frac{3}{4}(4 - K'_0)(R^{2/3} - 1) \right] \quad (2)$$

where $R = V_{T,0} / V_{T,P}$, $V_{T,0}$ is the volume at temperature and zero pressure (1 bar), $V_{T,P}$ is the volume at temperature and pressure, $K_{T,0}$ is the bulk modulus ($K_{T,0} = 1 / \beta_{T,0}$, where $\beta_{T,0}$ is the isothermal compressibility) at zero pressure, and K'_0 is the pressure dependence of the bulk modulus ($dK_{T,0} / dP$) at zero pressure.

Lange (2003) discussed the thermodynamic data used to calculate the fusion curve of albite and, based on a comparison with four previous experimental phase equilibria studies (Birch and LeComte, 1960; Boyd and England, 1963; Boettcher et al., 1982; and Nekvasil and Carroll, 1996), estimated that the K'_0 of $\text{NaAlSi}_3\text{O}_8$ liquid has a minimum value of 10. However, each experimental study lacked one or more key components essential to a robust determination of the fusion curve: (1) documentation of dissolved H_2O in their quenched glass run products; (2) a detailed thermal gradient and pressure calibration prior to experiments; and (3) characterization of crystalline starting material to be sure it was fully disordered, high albite. In order to tightly bracket the K'_0 value for liquid $\text{NaAlSi}_3\text{O}_8$, the goal of this study is to locate the fusion curve of albite in

P-T space through a series of piston-cylinder experiments, and address each component described above.

PREVIOUS WORK

Study of Birch and LeComte (1960)

The experiments of Birch and LeComte (1960) were performed in a gas vessel with argon gas as the pressure medium, thus allowing the pressure to be precisely and accurately known and minimizing H₂O in the system. Seven of their nine experiments had a starting material of crystalline albite; however, it is unclear if it was low or high albite. Anovitz and Blencoe (1999) noted that low albite will melt metastably at lower temperatures than high albite. All seven gave “no-reaction” results, which may be difficult to interpret. No reaction with a starting material of crystalline albite might mean that it was in the crystalline stability field at the P-T conditions of the experiment, or it might have remained crystalline because of sluggish kinetics. Run durations of these experiments ranged from 0.2 to 5.75 hours. The other two experiments by Birch and LeComte employed NaAlSi₃O₈ glass as the starting material. In these two runs, crystallization occurred within four and two hours, respectively, which constrains the melting temperature of albite to be $\geq 1210^{\circ}\text{C}$ at 1.22 GPa, and $\geq 1279^{\circ}\text{C}$ at 1.51 GPa.

Study of Boyd and England (1963)

The experiments of Boyd and England (1963) also provided constraints on the minimum temperatures for the albite fusion curve. The starting material was NaAlSi₃O₈ glass, and experiments were conducted with a 1.27 cm piston-cylinder apparatus using

talc/boron nitride as the pressure medium. Experimental run durations ranged from 20-60 minutes. Twenty-five degree brackets were determined at nominal pressures of 1.08 GPa (1225-1250°C), 1.79 GPa (1300-1325°C), 2.51 GPa (1350-1375°C), and 3.23 GPa (1400-1425°C) to constrain the half-reversal.

Talc/boron nitride (BN) assemblies require a pressure correction and the talc in the assembly dehydrates at high temperatures. Boyd and England (1963) carried out pressure calibrations at both room temperature and elevated temperatures. At room temperature, using bismuth, thallium, and cesium phase transitions, they found the friction, with the piston advancing, to be 13% of the nominal pressure. At elevated temperatures they used the quartz-coesite phase transition and determined the pressure correction to be 8% of the nominal pressure. Boyd and England (1963) noted that the furnace cells used for the quartz-coesite experiments contained a considerable amount of porous ceramic. Upon pressurization the porous ceramic collapsed, and the talc extruded into cracks and chips in the pressure vessel. Thus, the piston was continually advanced in order to maintain a constant pressure during their experiments.

However, they used a different cell assembly for the albite melting experiments where the ceramic pore volume was reduced, and noted that piston motion was reduced extensively after the first 1-2 minutes of their runs. They noted that based on the lack of piston advancement, their pressure correction was uncertain, and assumed no pressure correction for their experiments. However, Bohlen et al. (1980) later demonstrated through a pressure calibration against the melting curve of LiCl, that talc/BN assemblies require a 6% negative correction.

Talc/boron nitride assemblies also dehydrate at high temperatures, and hydrogen diffusion into platinum capsules will reduce the melting temperature of albite (Tuttle and Bowen, 1958). There was no documentation on how much water may have contaminated the experimental charges of Boyd and England (1963), which will depress the melting temperature. Therefore, only the experiments where the run products are crystalline can be used to constrain the minimum melting temperature of albite.

Study of Boettcher et al. (1982)

Boettcher et al. (1982) also determined the fusion curve of albite using a 1.27 cm diameter (for 3 GPa experiments) and a 2.54 cm diameter piston-cylinder apparatus. The advantages of their study are that full-reversals were determined and the crystalline starting material was well characterized. To avoid water contamination, their furnace assemblies contained no hydrous parts such as talc or pyrophyllite. Instead the assemblies consisted of KBr, NaCl, silica glass, and BN, which also had the advantage of having no pressure correction applied to the nominal pressure. The starting materials were sealed into 1.6 mm diameter platinum capsules which were surrounded by hematite and sealed into 3 mm platinum tubing to further prevent water contamination.

Experimental runs were 3-24 hours in duration. The results of Boettcher et al. (1982) place the melting curve of albite 50-70°C lower than the experiments of Birch and LeComte (1960) and Boyd and England (1963). The likely explanation for lower than expected results is that water contaminated their samples, despite their best efforts at keeping their runs dry. None of the samples of Boettcher et al. (1982) were directly

measured for water content, and two lines of evidence suggest water contamination occurred.

Fine and Stolper (1985) measured 0.20 wt% and 0.49 wt% H₂O on two albite glass samples supplied by A.L Boettcher. Boettcher synthesized the samples in a piston cylinder at 2.0 GPa for 1 and 3 hours at 1450°C with the same cell assembly and drying technique as that employed by Boettcher et al. (1982). Additionally, Fine and Stolper (1985) equilibrated NaAlSi₃O₈ liquid for one hour at 1450°C, and pressures ranging from 1.5 to 3.3 GPa using identical cell assemblies as those of Boettcher et al. (1982). The run products quenched to glasses with measured values of 0.14 to 0.89 wt% H₂O. Given the longer duration (3-24 hours) of the experiments by Boettcher et al. (1982), water concentrations may have exceeded those documented by Fine and Stolper (1985).

The second line of evidence is that most of the NaAlSi₃O₈ liquids from the high-pressure experiments of Boettcher et al. (1982) did not quench to a glass. To determine whether experiments were in the liquid field, Boettcher et al. (1982) used the distinct texture of albite crystals in sheaves or radial aggregates, which they identified as quench crystals from the liquid. This is in contrast to the findings of Birch and LeComte (1960), Boyd and England (1963), and Nekvasil and Carroll (1996), who all recovered glasses from their experiments and noted the ease with which albite liquid quenches to a glass. The presence of dissolved water in albite liquid will dramatically reduce its viscosity (Dingwell, 1987), which in turn aids nucleation.

Study of Nekvasil and Carroll (1996)

The most recent study of the albite melting reaction was performed by Nekvasil and Carroll (1996). Their experiments were performed in a piston-cylinder apparatus, with a BN/NaCl pressure medium. A pressure calibration using the anhydrous reaction $\text{Mg-cordierite} = \text{sapphirine} + \text{quartz}$ showed that no pressure correction is required. Samples containing crystalline albite as the starting material were held at a pressure of 1.13 GPa and 1400°C for 24 hours to ensure melting had occurred, before rapidly reducing the temperature to its final value. Experiments were then held for an additional 4 days. Four experiments were performed, and the results are as follows. At 1230 and 1240°C the run products were glass, whereas at 1200 and 1225°C the run products were crystalline. This constrains a five degree bracket of 1225-1230°C on the minimum melting temperature of albite, because the H₂O in their quenched glasses was not determined.

The bracket at 1.13 GPa is approximately 25°C higher than that of Boettcher et al. (1982) at a similar pressure. However, it is within the temperature brackets of Birch and LeComte (1960) as well as Boyd and England (1963). This study determined the melting curve at the relatively low pressure of 1.13 GPa, and does not place a tight constraint on the K'_0 for NaAlSi₃O₈ liquid at higher pressures.

EXPERIMENTAL METHODS

All experiments were carried out in a piston-cylinder apparatus with 1.27 cm diameter furnace assemblies and pistons. Figure 1 shows the BaCO₃-MgO-graphite furnace assembly. Temperature was measured with Pt/Pt₉₀Rh₁₀ (type S) thermocouple,

with an error of $\pm 2^\circ\text{C}$ over the temperature range of the experiments. No correction for the effect of pressure on emf was applied. Pressure was measured with a Heise gauge, which has an accuracy of $\pm 0.1\%$ of the measured pressure.

Hotspot determination and the thermal gradient across the sample capsule

The location of the hotspot and the thermal gradient across the length of the sample capsule were mapped out through seven sets of experiments where the temperature difference between two thermocouples was measured as a function of the distance from the base plug (Fig. 2). Twelve different setpoint temperatures were used, which ranged from 300-1400 $^\circ\text{C}$ with 100 degree intervals between each temperature. The nominal pressure ranged from 2.0 to 3.0 GPa. To allow two thermocouples to be placed a measured distance apart from one another, two holes of the 4-bore alumina tube were exposed by filing a measured distance from the tip (Fig. 3). For each experiment, the MgO rod and the MgO tube were cut to allow one of the two thermocouples to be located 14.1 mm from the base plug. This was always the “reference” thermocouple, which controlled the setpoint temperature. For each experiment, the pressure was taken to a nominal 2.0 GPa, the temperature ramp was temporarily halted at 100° intervals (from 300-1300 $^\circ\text{C}$), and the temperatures of the two thermocouples were recorded. At the highest temperature, (1391 $^\circ\text{C}$), the furnace assemblies were subjected to pressures ranging from 2.0 to 3.0 GPa (nominal), and it was found that pressure had no effect on the temperature difference measured between the two thermocouples.

A polynomial was fitted to the data from each temperature interval (Fig. 4), which had R^2 values ranging from 0.9996 to 1 (Appendix). From the curves, the hotspot was

located, and the temperature gradient was mapped across a sample capsule with an average length of 3.5 mm. (Fig. 5, Fig. 6). The data show that the hotspot shifts downward from 11.2 mm to 12.65 mm from the base plug with increasing temperature from 300-1200°C, but remains at 12.7 mm from 1300-1391°C. The temperature range of the albite experiments discussed below is 1290-1452°C, and therefore the hotspot was assumed to be located at 12.7 mm for all experiments. The assemblies were fabricated to allow the top of the capsules to be located at the hotspot. The temperature gradient is only 3.5°C across the upper third of the capsule, and an additional 30°C across the remaining two-thirds of the capsule. Therefore, the upper third of each experimental capsule was used to determine the albite melting curve in P-T space. The thermocouple was located 12 mm from the base plug, and read a nominal temperature 1.7°C lower than that at the hotspot. The uncertainty in temperature is estimated to be $\pm 4^\circ\text{C}$ for all experiments due to errors in calculating the thermal gradient, along with the error in type-S thermocouple.

Pressure calibration of the BaCO₃ assembly

To determine the friction correction for the BaCO₃-graphite furnace assembly at the experimental pressures, a pressure calibration using the melting curve of NaCl was performed. The starting material was reagent grade NaCl, which was ground dry in a mortar and pestle. The powder was packed into 3-millimeter diameter Pt capsules and heated at 450°C for ≥ 2 hours prior to sealing. The MgO in the assembly was heated at 1000°C for ≥ 12 hours prior to the experiments. A Pt₈₇Rh₁₃ sphere was placed at one end of each capsule, which was aligned at the top when placed into the assembly. At P-T

conditions in the NaCl crystalline stability field, the sphere remained at the top of the capsules, whereas at P-T conditions in the liquid stability field, the sphere fell to the bottom of the capsules. Experiments were 40 minutes in duration.

The results of the NaCl melting experiments are shown in Figure 7. Temperature brackets of seven and five degrees were determined at nominal pressures of 2.0 and 2.5 GPa, respectively. These results were then compared to the calculated melting curve of NaCl, using the thermodynamic data compiled by Lange (personal communication), and a K'_0 of 15.5 ± 0.5 for liquid NaCl obtained from a best fit to the melting curves of Clark (1959), Bohlen (1984), and Urakawa et al. (1999). The experimental results show that the actual pressure is $9 \pm 2\%$ lower than the nominal pressure. This matches the data from McDade et al. (2002) that showed a negative 9 percent correction for a similar 1.27 cm diameter BaCO₃ pressure medium, which is independent of temperature and pressure.

Synthesis and characterization of starting material

The NaAlSi₃O₈ glass used in these experiments was synthesized by Ochs and Lange (1997). The wet chemical analysis of that glass is given in Figure 8. Crystalline albite was synthesized from the NaAlSi₃O₈ glass in a piston-cylinder apparatus. Three 5 mm diameter Pt capsules were packed with glass, and synthesis was performed at 1.82 GPa (A108 and A114) and 2.73 GPa (M130) at temperatures $\sim 75^\circ\text{C}$ below the albite melting curve. The run products were taken out of the capsules, powdered, and analyzed by XRD to confirm the material was high albite (Fig. 9).

The NaAlSi₃O₈ glass to crystalline albite reaction

For the glass to crystalline reaction, NaAlSi₃O₈ glass was mechanically powdered and packed into 3 mm diameter Pt capsules. The capsules were coned nearly shut, and placed in a furnace for ≥ 12 hours at 750°C. After heating they were placed in a vacuum bell jar to cool. The capsules were then immediately coned shut, spot welded, and shaped into cylinders. The MgO was heated at 1000°C for ≥ 12 hours prior to experiments. The BaCO₃ cells were stored in a 150°C furnace before they were needed. Experiments were raised to roughly 10% below the desired pressure before the temperature was ramped up to the desired value. Once the final temperature was reached, the pressure was increased to its desired value. The runs ranged from 40 to 50 minutes, and during their entirety experienced a constant increase in pressure, even though the oil supply was shut off and no leaking was visible in the system. In order to keep the pressure stable, the valve on the lower ram was opened every time the pressure was 0.005 GPa above the desired value and the pressure was dropped to 0.005 GPa below the desired value. The valve was then left partially open to slow the pressure increase. This needed to be repeated 5 or 6 times over the course of each run. The same pressure conditions occurred during the NaCl pressure calibration.

The crystalline albite to NaAlSi₃O₈ glass reaction

Before the crystalline to glass half-reversal experiments could be done at the University of Michigan, the pressure vessel became too cracked and chipped to continue being used. In an attempt to provide a full reversal on the crystal-liquid reaction, six experiments with crystalline, high albite as the starting material were carried out in the

experimental petrology laboratory at the University of Minnesota, under the supervision of M. M. Hirschmann. A -6% pressure correction was applied to the BaCO₃-MgO-graphite assembly, which had been previously determined with quartz-coesite experiments. However the pressure vessel conditions had changed from brand new at the time of the pressure calibration, to having four cracks down the bore when the crystalline to glass half-reversal experiments were performed, which may have changed the pressure correction. The hotspot was assumed to be 13 mm below the base plug, based on of a two-pyroxene temperature calibration on another piston-cylinder apparatus in the laboratory. Therefore, the exact errors associated with the pressure and temperature measurements are unknown. The cell assemblies were prepared as they were for the experiments at the University of Michigan, with the exception that the starting material was crystalline, high albite. The runs were pressurized first, and the temperature was raised to roughly 100 degrees below the final temperature. The pressure was then increased to its final value, and the temperature ramp was resumed until it reached its final temperature. The runs were held for 45 minutes, and the pressure remained constant for the duration of the experiments.

H₂O analysis of quenched NaAlSi₃O₈ glass

Run products that quenched to glass were mounted in epoxy, doubly polished, and analyzed by a Perkin-Elmer Spectrum GX Fourier Transform Infra-red (FTIR) spectrometer to determine the absorbance of the samples. The water concentrations were determined with the Beer-Lambert Law equation:

$$\text{Abs}_{3570} = C_{\text{H}_2\text{O}} \cdot d \cdot \rho \cdot \epsilon_{3570} / 18.0152 \quad (3)$$

where Abs_{3570} is the absorbance at 3570 cm^{-1} band, $C_{\text{H}_2\text{O}}$ is the weight fraction of total water, d is the sample thickness, ρ is the albite glass density, and ϵ_{3570} is the molar absorptivity. A value of $70.00 \pm 2.0 \text{ L/mol}\cdot\text{cm}$ was used for the molar absorptivity (Mandeville et al., 2002). Samples ranged from 0.98-1.02 mm in thickness. It is almost certain that the density of the quenched $\text{NaAlSi}_3\text{O}_8$ glass increased with the pressure of the piston-cylinder experiments owing to compression. When all else is equal, the effect of increasing the glass density is to reduce the calculated water concentration from the Beer-Lambert Law equation. Therefore, maximum water concentrations were calculated for the glasses quenched from the piston-cylinder experiments by using the density for $\text{NaAlSi}_3\text{O}_8$ glass synthesized at one bar (2.62 g/cm^3 ; Ochs and Lange, 1997).

RESULTS

Figures 10, 11, and 15 show the phase-equilibrium results from this study. Ten and five degree brackets were obtained for the glass to crystal reaction at 2.28 GPa (1360-1370°C) and 2.73 GPa (1385-1389°C), respectively. The run products had three distinct textural features (Fig. 12-14), which determined where they were located with respect to the fusion curve: (1) clear glass, (2) semi-transparent, and (3) white and opaque. Samples equilibrated in the liquid stability field quenched to a clear glass (top of A72, A50, and A60). The top of sample A65 (Fig. 13) also contained clear glass, but albite crystals were present throughout it. Samples held at P-T conditions slightly below the fusion curve quenched to a semi-transparent texture (A57, bottoms of A65, A72, and A50); under a microscope it was seen that very small (30-5 μm) crystals had formed. At temperatures well below the fusion curve, a white, opaque texture was formed from

larger (650-100 μm) albite crystals (A52 and A54). Runs A72, A50, and A60 show the progression of glass to crystal through the thermal gradient, and they show the ease with which albite quenches to a glass.

Additionally, a 10° bracket was obtained for the crystal to liquid reaction at 2.73 GPa (1389-1399 $^\circ\text{C}$) from the experiments at the University of Minnesota (Fig. 10, Fig. 15). The run products had similar textural features as those described above, with the exception that the quenched glasses contained small ($50 \times 50 \mu\text{m}$) crystals. These samples were analyzed using the SEM at the University of Michigan, and it was seen that periclase (MgO) is present (Fig. 16). This is likely due to contamination of MgO from the cell assembly (Fig. 1) when the crystalline albite (synthesized in the piston-cylinder apparatus) was extracted from the Pt capsules. Analysis by electron dispersive spectroscopy (EDS) shows that some of the MgO dissolved into the $\text{NaAlSi}_3\text{O}_8$ liquid (Fig. 17b, Fig. 17c), but it was not incorporated into the crystalline albite (Fig. 17a). The one-bar ternary diagram of Schairer (1957) provides two analogues on the effect that MgO has on the melting temperature of albite using $2\text{MgO}\cdot 2\text{Al}_2\text{O}_3\cdot 5\text{SiO}_2$ (cordierite) and $2\text{MgO}\cdot \text{SiO}_2$ (forsterite). The effect is a reduction in temperature of $\sim 2^\circ\text{C}$ and $\sim 3^\circ\text{C}$ (with an error of $\pm 3^\circ\text{C}$), respectively, when the one-atm melting temperature of albite is corrected from 1118°C to 1100°C (Boettcher et al., 1982). The presence of MgO in the samples, coupled with the uncertainty in the pressure correction and thermal gradient, reduces the reliability of these results when compared to the experiments performed at the University of Michigan. Nonetheless, inter-laboratory agreement for the albite melting temperature at 2.7 GPa is within $\sim 5\text{-}14^\circ\text{C}$ between the results from the University

of Minnesota (crystal to liquid), and those from the University of Michigan (glass to crystal).

Glass run products obtained from both sets of experiments (University of Michigan and University of Minnesota) were analyzed for water using FTIR spectroscopy (Fig. 10). Concentrations ranged from 0.006 wt% to 0.045 wt% H₂O (60-450 ppm).

DISCUSSION

Constraints on the K'_0 of NaAlSi₃O₈ liquid

The experimental results (Fig. 10), which bracket the location of the albite fusion curve in P-T space, are superimposed on a family of calculated fusion curves in Figure 11 for different K'_0 values for NaAlSi₃O₈ liquid, using the 3rd-order Birch-Murnaghan EOS. The phase equilibrium constraints at 2.28 and 2.73 GPa tightly constrain the value for the liquid K'_0 to be 10.7 ± 0.5 . The uncertainty of ± 0.5 units is obtained from the uncertainties in the temperature brackets (10° at 2.28 GPa and 8° at 2.73 GPa, respectively) and the uncertainty in the negative pressure correction ($9 \pm 2\%$). With this calculated fusion curve in hand, for a liquid K'_0 of 10.7 ± 0.5 , a comparison with all previous work can be made at all experimental pressures.

Comparison with previous work

A comparison between the results of this study (Fig. 10, Fig. 11) and those of Birch and LeComte (1960) (Fig. 18) resolves the two questions regarding their experimental data. The first is whether their no-reaction experiments with a starting

material of crystalline albite were a result of sluggish kinetics. The second is whether their crystalline starting material was low or high albite. The present results at temperatures $\geq 1272^{\circ}\text{C}$ demonstrate that crystalline albite melts and that albite crystallizes readily from a glass (or liquid) within 45 minutes or less. Therefore, the “no-reaction” experiments of Birch and LeComte (1960) conducted at 2.29 and 1.92 GPa (both at temperatures $> 1300^{\circ}\text{C}$), which that lasted more than 45 minutes, can be confidently interpreted as P-T conditions within the crystalline stability field. In addition, there is no evidence that the results of Birch and LeComte (1960) reflect metastable melting of low albite at temperatures lower than those for high albite. To the contrary, the temperature brackets provided by Birch and LeComte (1960) for the albite fusion curve are among the highest in temperature compared to previous studies and match this study (where high albite was confirmed). In addition, the excellent agreement between the results from this study and those from Birch and LeComte (1960), which had excellent pressure control owing to the gas pressure medium, provides an independent verification on the pressure calibration of this study.

Our results are also consistent with those of Boyd and England (1963), especially when the negative 6 % pressure correction for talc/BN assemblies documented by Bohlen et al. (1980) are applied to the Boyd and England results. This leads to revised pressures of 1.02, 1.68, 2.36, and 3.04 GPa for temperature brackets of 1225-1250 $^{\circ}\text{C}$, 1300-1325 $^{\circ}\text{C}$, 1350-1375 $^{\circ}\text{C}$, and 1400-1425 $^{\circ}\text{C}$, respectively, that tightly fit the fusion curve calculated for a liquid K'_0 of 10.7 ± 0.5 (Fig. 19). The experiments of Boyd and England likely had minimal H₂O contamination, considering the short run durations (20-

60 min) of their experiments and the ease with which their NaAlSi₃O₈ liquid quenched to a glass.

Figure 13 shows the results of Boettcher et al. (1982) superimposed on the calculated family of fusion curves in Figure 20. There is no liquid K'_0 value that matches their results. The results of Boettcher et al. (1982) at 2.5 and 3.0 GPa are ~65 and ~53°C lower than calculated for the fusion curve with a liquid K'_0 of 10.7. Lange (2003) provides an equation that allows the amount of water required to suppress the albite melting temperature a known amount to be calculated. From equation (10) in that paper, the results of Boettcher et al. (1982) at 2.5 and 3.0 GPa appear to have contained ~0.73 and ~0.95 wt % H₂O, which is consistent with the range of H₂O estimated for their samples (equilibrated for 3-24 hours) on the basis of the H₂O measurements reported in Fine and Stolper (1985).

Figure 20 also shows the results of Nekvasil and Carroll (1996) at 1.1 GPa, which are ~35°C lower than that calculated for the albite fusion curve with 10.7 for the liquid K'_0 value. This discrepancy may be due to small amounts of H₂O (~0.4 wt %) infiltrating their samples, which is plausible given their long (5 day) experiments.

The density of NaAlSi₃O₈ liquid as a function of pressure

With tight constraints on the value of K'_0 for NaAlSi₃O₈ liquid, its molar volume (or density) can be calculated to high pressure with the third-order Birch-Murnaghan EOS (eq. 2). The one-bar liquid volume, thermal expansivity and compressibility are obtained from Lange (1996) and Kress et al. (1988). In Figure 22, the molar volume of NaAlSi₃O₈ liquid is calculated as a function of pressure at 1500 °C to 3.3 GPa for various

liquid K'_0 values. The volume vs. pressure curve for a liquid K'_0 of 10.7 is highlighted relative to those calculated for K'_0 values of 4, 6, 8, and 12. Also shown is the density of crystalline albite calculated from the data of Wruck et al. (1991), Fei (1995), and Downs et al. (1994). The liquid volume remains greater than that for crystalline albite to 3.3 GPa, which is why the fusion curve maintains a positive dT/dP slope. An uncertainty in the K'_0 value of ± 0.5 contributes an error of $\pm 0.2\%$ to the liquid density at 1500 °C and 3 GPa ($2.546 \pm 0.004 \text{ g/cm}^3$). If this calculation is extended to 1500 °C and 8 GPa, the uncertainty is $\pm 0.5\%$ ($2.773 \pm 0.015 \text{ g/cm}^3$).

The density of the liquid can also be calculated along the fusion curve at various P-T conditions. The results of this study allow the percent deviation in liquid density at 3.3 GPa to be calculated for different liquid K'_0 values. These results show that an error in liquid density of $\sim 3.6\%$ will lead to an error in the calculated temperature of the fusion curve of $\sim 105 \text{ °C}$ (Fig. 21).

The compressibility of NaAlSi₃O₈ liquid as a function of pressure

It is of interest to examine not only variation of the density of liquid NaAlSi₃O₈ with pressure for different K'_0 values, but also variation of the compressibility. Its variation with pressure is calculated from the equation:

$$\beta_T(P) = \frac{1}{K_T(P)} = -\frac{1}{V_T(P)} \left[\left(\frac{\partial P}{\partial V} \right)_T \right]^{-1} \quad (4)$$

where $(\partial P / \partial V)_T$ is the derivative of equation 2 with respect volume:

$$\left(\frac{\partial P}{\partial V}\right)_T = \frac{3}{4} \frac{K_{T,0}}{V_{T,0}} (R^{7/3} - R^{5/3}) (4 - K') R^{5/3} + \frac{3}{2} \frac{K_{T,0}}{V_{T,0}} \left(\frac{5}{3} R^{8/3} - \frac{7}{3} R^{10/3} \right) \left(1 - \frac{3}{4} (4 - K') (R^{2/3} - 1) \right) \quad (5)$$

The resultant β_T vs P curves at 1500°C (Fig. 23) show that for a K'_0 value of 10.7 ± 0.5 at 1500°C there is a pronounced curvature, with β_T rapidly decreasing at low pressure. In contrast, a low K'_0 value of 4 (commonly assumed for magmatic liquids) leads to a less sharp decrease in β_T with P. At 1500°C, for a K'_0 value of 10.7, the liquid has a compressibility at one bar ($\sim 5.8 \times 10^{-6} \text{ bars}^{-1}$) that is > 320 % greater than that for crystalline albite ($\sim 1.8 \times 10^{-6} \text{ bars}^{-1}$). By 3 GPa, the difference between the liquid and crystalline compressibility is only $0.9 \times 10^{-6} \text{ bars}^{-1}$ ($\sim 2.3 \times 10^{-6} \text{ bars}^{-1}$ vs. $\sim 1.4 \times 10^{-6} \text{ bars}^{-1}$), and by 8 GPa the difference is only $0.2 \times 10^{-6} \text{ bars}^{-1}$ ($\sim 1.3 \times 10^{-6} \text{ bars}^{-1}$ vs. $\sim 1.1 \times 10^{-6} \text{ bars}^{-1}$) (Fig. 23). These results illustrate that at 1500 °C and one bar, there are mechanisms of compression available to liquid NaAlSi₃O₈ that are not accessible to its crystalline equivalent. Moreover, these mechanisms of compression are rapidly lost with increasing pressure between 0 and 8 GPa.

Topological mechanisms of compression for liquid NaAlSi₃O₈

There are two broad mechanisms of compression by which the molar volume of multi-component silicate liquids may change with increasing pressure. One involves coordination change (4 vs. 5 vs. 6) of network-forming cations (e.g., Al³⁺, Si⁴⁺), whereas the other is topological and may involve changes in Qⁿ speciation, T-O-T bond angles,

and network connectivity, such as the occurrence of clusters and/or changes in the size distribution of rings of tetrahedra. For example, Stixrude and Bukowinski (1990a) demonstrated that topological variations in network connectivity can exert a strong influence on melt density. Using Monte-Carlo simulations of tetrahedrally bonded SiO₂ liquid at various pressures, they showed that SiO₂ melt compresses by reducing the abundance of three-membered rings in favor of larger-sized rings and a broader distribution of the size of rings. These conclusions are consistent with the strong variations in density (factor of 2) observed in crystalline frameworks as a systematic function of ring statistics (Stixrude and Bukowinski, 1990b), where decreasing ring size leads to lower density. A broader distribution of larger ring sizes allows a more efficient packing of tetrahedral units. The gradual increase in ring size seen in the simulated liquids with pressure is achieved only because Si-O bonds are constantly broken and reformed; therefore, it is a compression mechanism uniquely available to liquids and not crystals. This may be an important topological mechanism for the compression of fully polymerized NaAlSi₃O₈ liquid at pressures ≤ 8 GPa, where neither Si⁴⁺ nor Al³⁺ undergoes a coordination change (Lee et al., 2004).

CONCLUSIONS

The phase equilibrium results on the fusion curve of albite presented in this study closely matches the data of Birch and LeComte (1960) and the pressure corrected data of Boyd and England (1963). This study demonstrates that well-determined experimental constraints on the albite melting reaction, when combined with thermodynamic analysis of the fusion curve, allows the density and compressibility of this viscous, fully polymerized liquid to be calculated to high pressure with a remarkably high precision and

accuracy. A 3rd order Birch-Murnaghan equation of state and a K_0' value of 10.7 for liquid NaAlSi₃O₈ can be applied up to ~8 GPa, owing to the absence of any coordination change and the dominance of topological mechanisms of compression in this liquid between 0 and 8 GPa.

ACKNOWLEDGEMENTS

The author thanks Marc Hirschmann, Tony Withers, and the experimental petrology group at the University of Minnesota for use of their laboratory at such short notice. He also thanks Eric Essene for many discussions and for the review of the thesis. This research was supported by the National Science Foundation (EAR-0310079).

REFERENCES

- Anovitz, L.M. and Blencoe, J.G. (1999) Dry melting of albite. *American Mineralogist*, 84, 1830–1842.
- Birch, F. (1978) Finite strain isotherm and velocities for single-crystal and polycrystalline NaCl at high pressure and 300 K. *Journal of Geophysical Research*, 83, 1257–1268.
- Birch, F. and LeComte, P. (1960) Temperature-pressure plane for albite composition. *American Journal of Science*, 258, 209–217.
- Boettcher, A.L., Burnham, C.W., Windom, K.E., and Bohlen, S.R. (1982) Liquids, glasses and the melting of silicates to high pressures. *Journal of Geology*, 90, 127–138.

- Bohlen, S.R. (1984) Equilibria for precise pressure calibration and a frictionless furnace assembly for the piston-cylinder apparatus. *Neues Jahrbuch für Mineralogie. Monatshefte*, 4, 404–412.
- Bohlen, S.R., Essene, E.J., and Boettcher, A.L. (1980) Reinvestigation and application of olivine-quartz-orthopyroxene barometry. *Earth and Planetary Science Letters*, 47, 1–10.
- Boyd, F.R. and England, J.L. (1963) Effect of pressure on the melting of diopside, $\text{CaMgSi}_2\text{O}_6$, and albite $\text{NaAlSi}_3\text{O}_8$, in the range up to 50 kilobars. *Journal of Geophysical Research*, 68, 311–323.
- Dingwell, D.B. (1987) Melt viscosities in the system $\text{NaAlSi}_3\text{O}_8$ - H_2O - F_2O . In B.O. Mysen, Ed., *Magmatic Processes: Physiochemical Principles*, 433 p. The Geochemical society Special Publications.
- Downs, R.T., Hazen, R.M., and Finger, L.W. (1994) The high-pressure crystal chemistry of low albite and the origin of the low pressure dependency of Al-Si ordering. *American Mineralogist*, 79, 1042–1052
- Fei, Y. (1995) Thermal expansion. In T. Ahrens, Ed., *Mineral Physics and Crystallography*, p. 29–44. AGU Reference Shelf 2, Washington, D.C.
- Fine, G. and Stolper, E. (1985) The speciation of carbon dioxide in sodium aluminosilicate glasses. *Contributions to Mineralogy and Petrology*, 91, 105–121.
- Holland, T.J.B (1980) The reaction albite = jadeitite + quartz determined experimentally in the range 600-1200 °C. *American Mineralogist*, 65, 129–134.
- Kress, V.C., Williams, Q., and Carmichael, I.S.E. (1988) Ultrasonic investigation of melts in the system Na_2O - Al_2O_3 - SiO_2 liquids between 701 and 1896 K: extension to

crustal magmatic temperatures. *Contributions to Mineralogy and Petrology*, 130, 1–11.

Lange, R.A. (2003) The fusion curve of albite revisited and the compressibility of NaAlSi₃O₈ liquid with pressure. *American Mineralogist*, 88, 109–120.

Lee, S.K., Cody, G.D., Fei, Y., and Mysen, B.O. (2004) Nature of polymerization and properties of silicate melts and glasses at high pressure. *Geochimica et Cosmochimica Acta*, 68, 4189–4200

Mandeville, C.W., Webster, J.D., Rutherford, M.J., Taylor, B.E., Timbal, A., and Faure, K. (2002) Determination of molar absorptivities for infrared absorption bands of H₂O in andesitic glasses. *American Mineralogist*, 87, 813–821.

McDade, P., Wood, B.J., Van Westrenen W., Brooker, R., Gudmundsson, G., Soulard, H., Najorka, J., and Blundy, J. (2002) Pressure corrections for a selection of piston-cylinder cell assemblies. *Mineral Magazine*, 66, 1021–1028.

Nekvasil, H. and Carroll, W. (1996) Experimental constraints on the compositional evolution of crustal magmas. *Transactions of the Royal Society of Edinburgh: Earth Sciences*, 87, 139–146.

Ochs III, F.A. and Lange, R.A. (1997) The partial molar volume, thermal expansivity, and compressibility of H₂O in NaAlSi₃O₈ liquid: New measurements and an internally consistent model. *Contributions to Mineralogy and Petrology*, 129, 155–165.

Pickering J.M., Schwab B.E., Johnston A.D. (1998) Off center hotspots: Double thermocouple determination of the thermal gradient in a 1.27 cm (1/2 in.) CaF₂ piston-cylinder furnace assembly. *American Mineralogist*, 83, 228–235.

- Schairer, J.F. (1957) Carnegie Inst. Washington, Yearbook, 56, 219.
- Stixrude, L. and Bukowinski, M.S.T. (1990) Fundamental thermodynamic relations and silicate melting with implications for the constitution of D''. Journal of Geophysical Research, 95, 19311–19327
- Stixrude, L. and Bukowinski, M.S.T. (1990) Rings, topology, and the density of tectosilicates. American Mineralogist, 75, 1159–1169.
- Tuttle, O.F., and Bowen, N.L. (1958) Origin of granite in the light of experimental studies in the NaAlSi₃O₈-KAlSi₃O₈-SiO₂-H₂O. Geological Society of America Memoir, v. 74, 1–153.
- Urakawa, S., Igawa, N., Shimomura, O., and Ohno, H. (1999) High-pressure X-ray diffraction on the study of NaCl melt using synchrotron radiation. American Mineralogist, 84, 341–344.
- Wruck, B., Salje, E.K.H., Graeme-Barber, A. (1991) Kinetic rate laws derived from order parameter theory IV: kinetics of Al, Si, disordering in Na-feldspars. Physics and Chemistry of Minerals, 17, 700–710.

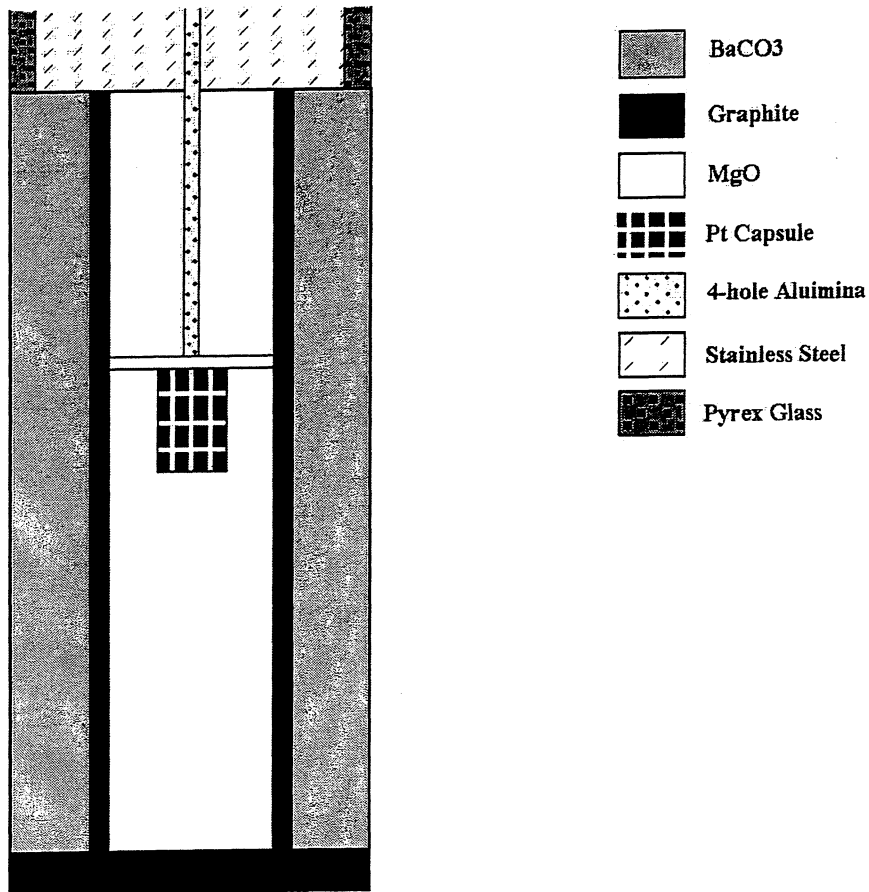


Figure 1. BaCO₃/MgO/graphite 1.27 cm diameter assembly. The assembly dimensions are as follows: BaCO₃ length: 30 mm; graphite furnace length: 30 mm; solid MgO length: 17.5 mm; MgO disk: 0.5 mm; drilled MgO length: 12 mm; capsule length: ~3.5 mm; capsule width: ~3 mm. The University of Minnesota assembly dimensions are as follows: BaCO₃ length: 32 mm; graphite furnace length: ~31.8 mm; solid MgO length: 19 mm; MgO disk: 1 mm; drilled MgO length: 12 mm; capsule length: ~3.5 mm; capsule width: ~3 mm. Separate thermal gradients and pressure corrections were determined for each assembly.

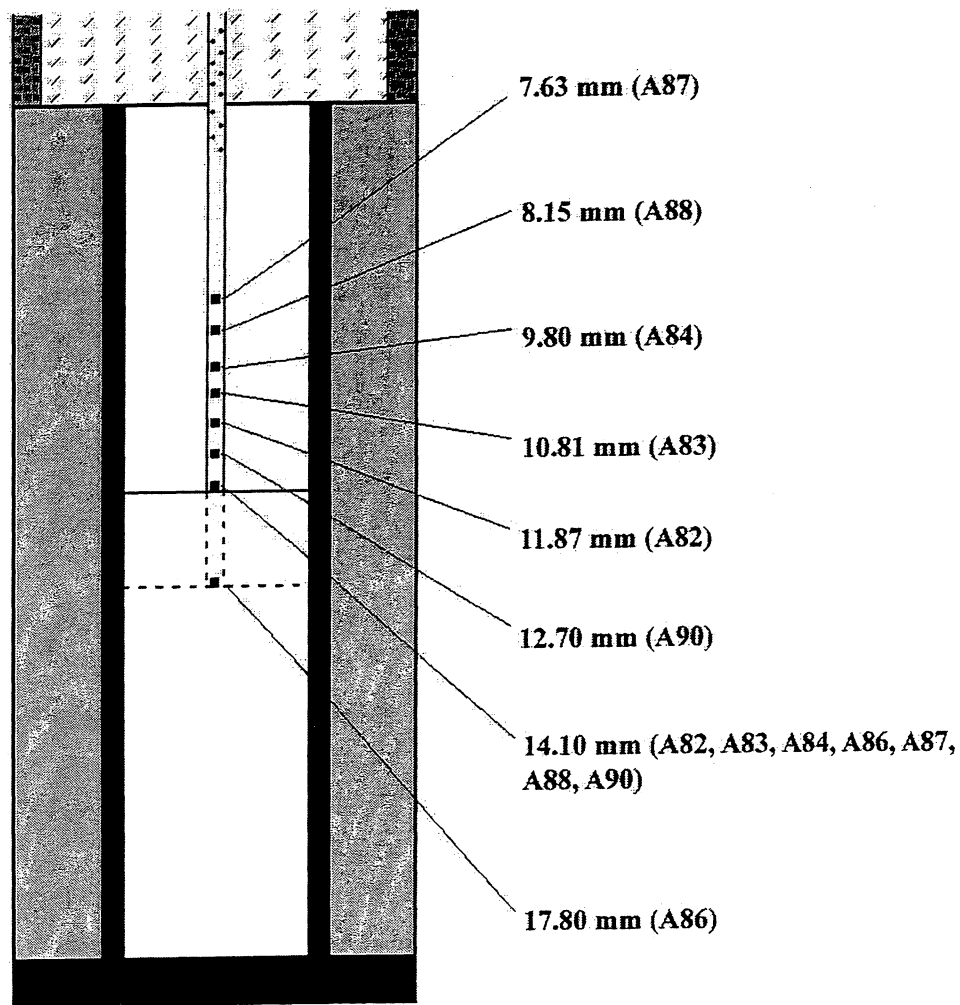


Figure 2. Thermocouple locations used to determine the hotspot and thermal gradient on the piston-cylinder. All locations are measured prior to experimental conditions. For experiments A82, A83, A84, A87, A88, and A90, the drilled MgO was 14.10 mm in length, while the solid MgO was 15.90 mm in length. The thermocouples located at 14.10 mm controlled the temperature while the second thermocouples measured the temperature difference relative to 14.10 mm. For experiment A86 the drilled MgO was 17.80 mm in length, while the solid MgO was 12.2 mm in length. The thermocouple located at 14.10 controlled the temperature, while the thermocouple located at 17.80 mm measured the temperature difference relative to 14.10 mm.

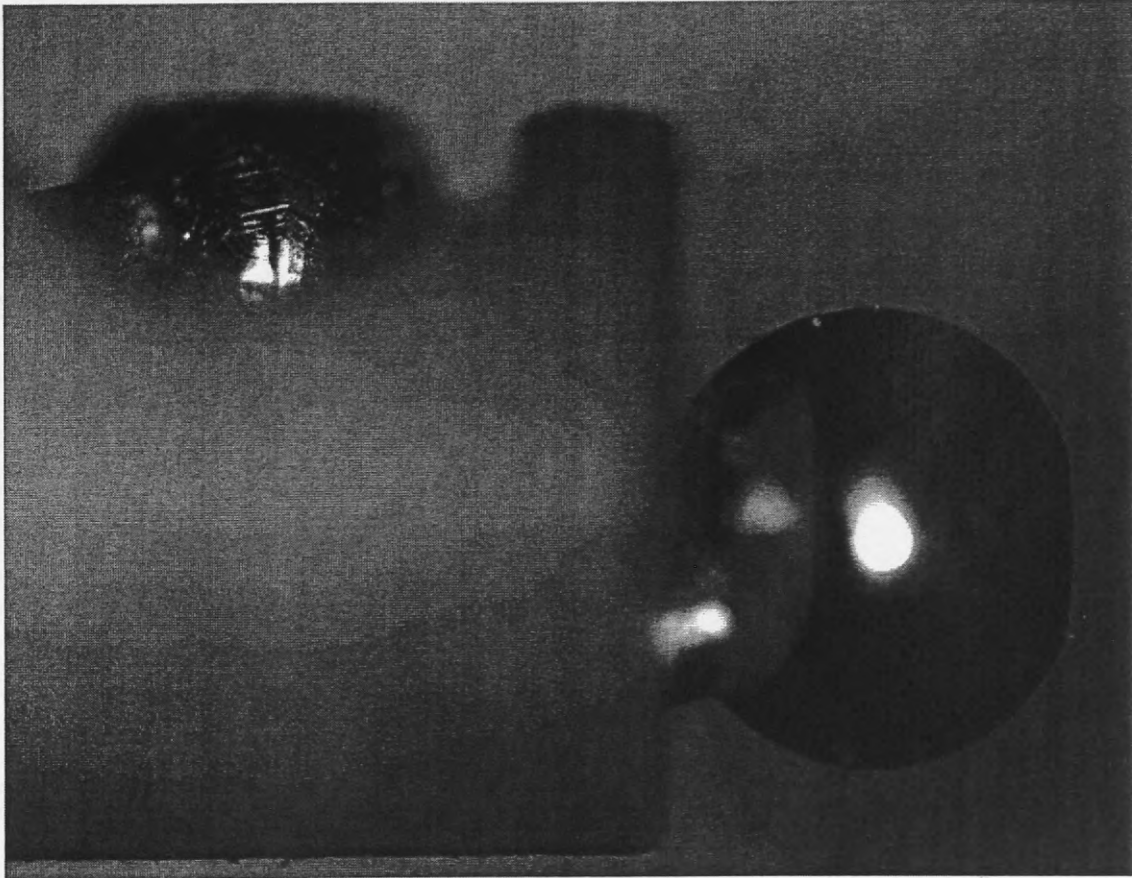


Figure 3. Image of experiment A90 2-thermocouple assembly. The image shows the 2 thermocouple junctions at a fixed distance of 1.40 mm from the tip-to-tip of each sphere.

Experiment	Distance From Base Plug, mm	Temperature, C
A87	7.63	1151.5
A88	8.15	1258
A84	9.8	1369
A83	10.81	1387
A82	11.87	1393
A90	12.7	1398.5
A82, A83, A84, A86, A87, A88, A90	14.1	1391
A86	17.8	1304.5

Figure 4. 1391° data from the hotspot experiments.

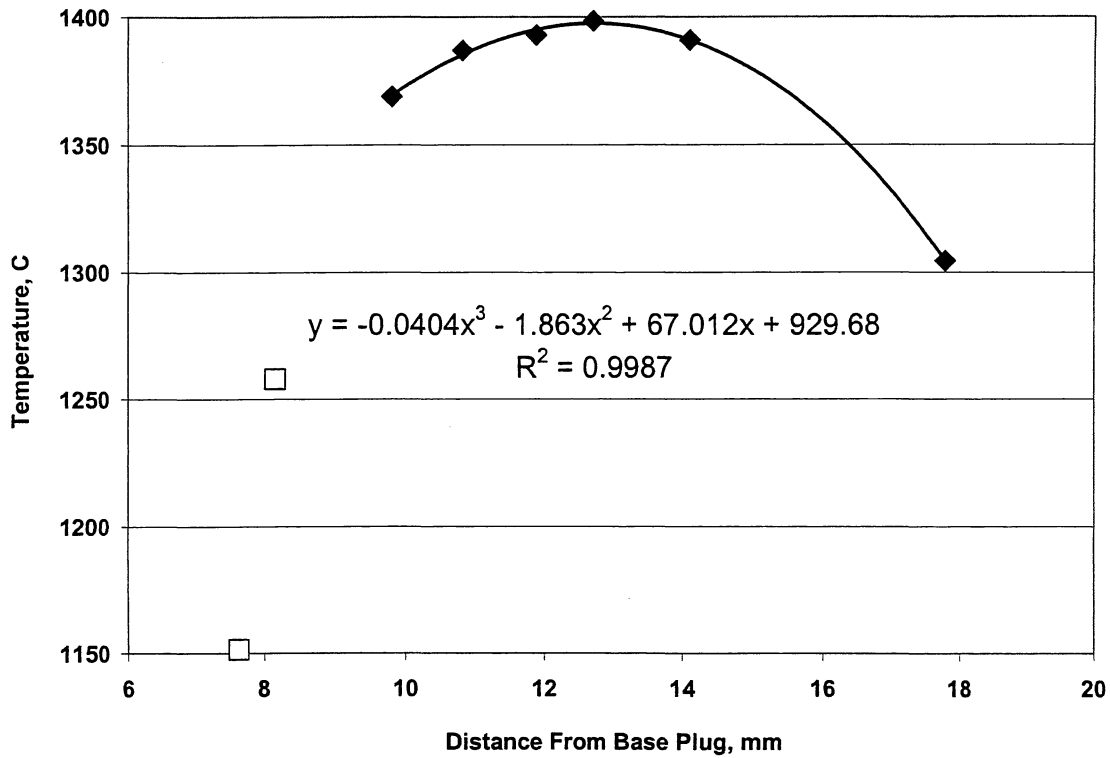


Figure 5. A graphical plot of the data from Table 1, showing the polynomial best fit curve. Open squares (experiments A87 and A88) are left off the best fit curve, and show the asymmetry in the thermal gradient of the 1.27 cm assembly.

Temperature difference from hotspot, (°C)	Distance From Base Plug, mm
-1.7	12
-0.8	12.25
-0.2	12.5
0.0	12.7
-0.2	13
-0.9	13.25
-2.0	13.5
-3.4	13.73
-5.5	14
-7.9	14.25
-10.8	14.5
-13.8	14.73
-17.8	15
-22.1	15.25
-26.7	15.5
-33.0	15.8
-37.5	16

Figure 6. Thermal gradient and hotspot calculated from the polynomial equation $T(^{\circ}\text{C}) = -0.0404x^3 - 1.863x^2 + 67.012x + 929.68$ (Figure 5). x = distance below the base plug, mm. The hotspot is calculated at 12.7 mm from the base plug, and the temperature difference from the hotspot is shown.

Experiment	Pressure (nominal), GPa	Temperature, °C	Pt/Rh sphere position
A51	2.0	1123	Top
A55	2.0	1131	Top
A53	2.0	1138	Bottom
A49	2.0	1146	Bottom
A48	2.0	1153	Bottom
A48	2.0	1153	Bottom
A119	2.5	1187	Top
A121	2.5	1192	Bottom
A120	2.5	1197	Bottom
A118	2.5	1202	Bottom
A117	2.5	1212	Bottom
A116	2.5	1217	Bottom

Figure 7. Results of NaCl melting experiments used to determine the pressure correction of the BaCO₃/Graphite assembly. Based off the NaCl fusion curve of Lange (2005), the 2.0 nominal GPa experiments determine a pressure correction of $-7.8\% \pm 1.3\%$, and the 2.5 nominal GPa experiments determine a pressure correction of $-10.9\% \pm 0.70\%$. The pressure correction used for the albite experiments is $-9\% \pm 2\%$ based on these results.

Oxide	Analysed composition		Ideal albite (mol%)
	Measured (wt%)	Normalized (mol%)	
SiO ₂	68.5	74.99	75.00
Al ₂ O ₃	19.42	12.53	12.50
Na ₂ O	11.76	12.48	12.50
H ₂ O	0.22	x	x
Total	99.68	100	100

Figure 8. NaAlSi₃O₈ starting glass composition (Ochs and Lange, 1997)

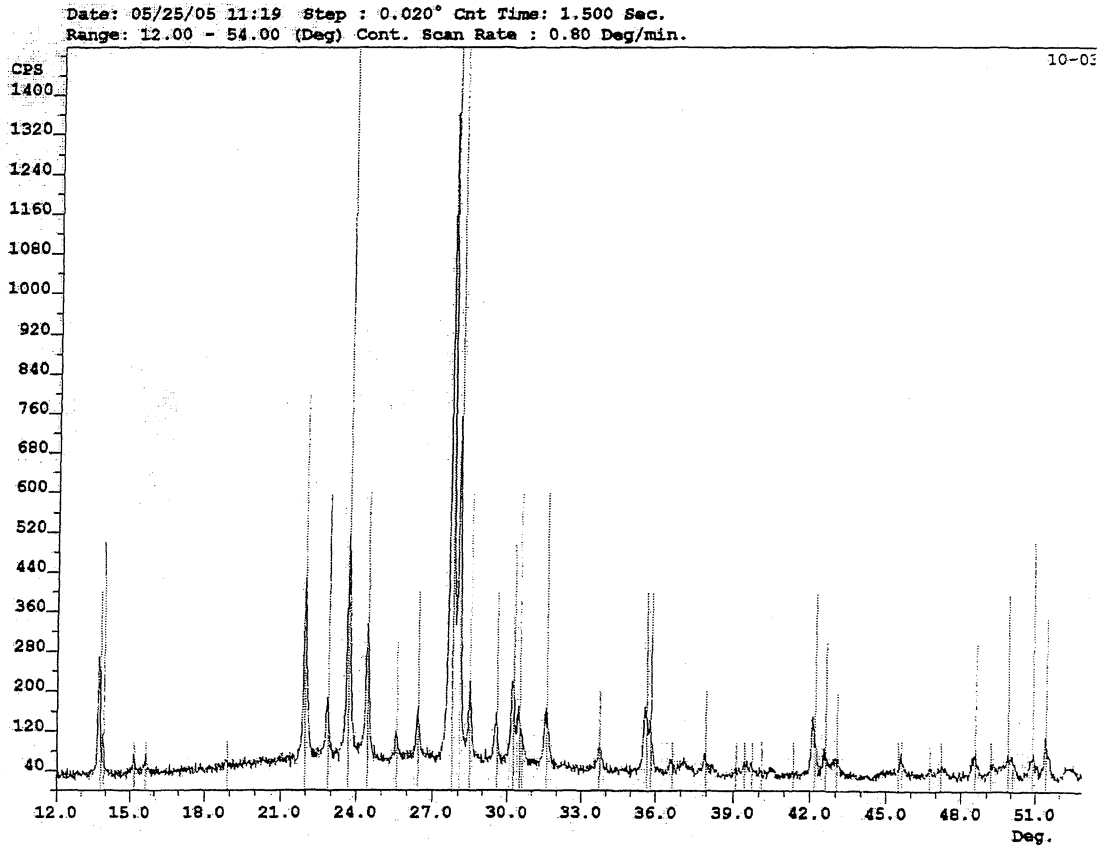


Figure 9. XRD peaks of crystalline synthesis products. Solid lines represent the location of the albite peaks. Experiments M130, A108, and A114 had the same peaks.

Experiment	Pressure (nominal), GPa	Pressure (corrected), GPa	Temperature, C	Starting Material	Run Product	wt. % H2O	XRD
A52	3.0	2.73	1290	Glass	Xtl		
A54	3.0	2.73	1340	Glass	Xtl		
A57	3.0	2.73	1370	Glass	Xtl		
A65	3.0	2.73	1385	Glass	Xtl		
A72	3.0	2.73	1389	Glass	Glass	0.01	
A50	3.0	2.73	1402	Glass	Glass	0.045	
A60	3.0	2.73	1452	Glass	Glass	0.006	
M130	2.89	2.73	1311	Xtl	Xtl		Yes
M129	2.89	2.73	1389	Xtl	Xtl		
M132	2.89	2.73	1389	Xtl	Xtl		
M133	2.89	2.73	1399	Xtl	Glass		
M131	2.89	2.73	1419	Xtl	Glass		
M134	2.89	2.73	1475	Xtl	Glass	0.03	
A74	2.5	2.275	1352	Glass	Xtl		
A73	2.5	2.275	1360	Glass	Xtl	0.01	
A75	2.5	2.275	1370	Glass	Glass	0.01	
A76	2.5	2.275	1378	Glass	Glass		
A77	2.5	2.275	1378	Glass	Glass		
A108	2.0	1.82	1272	Glass	Xtl		Yes
A114	2.0	1.82	1300	Glass	Xtl		Yes

Figure 10. Results of all albite fusion curve experiments. Temperature brackets at pressure are shown in bold.

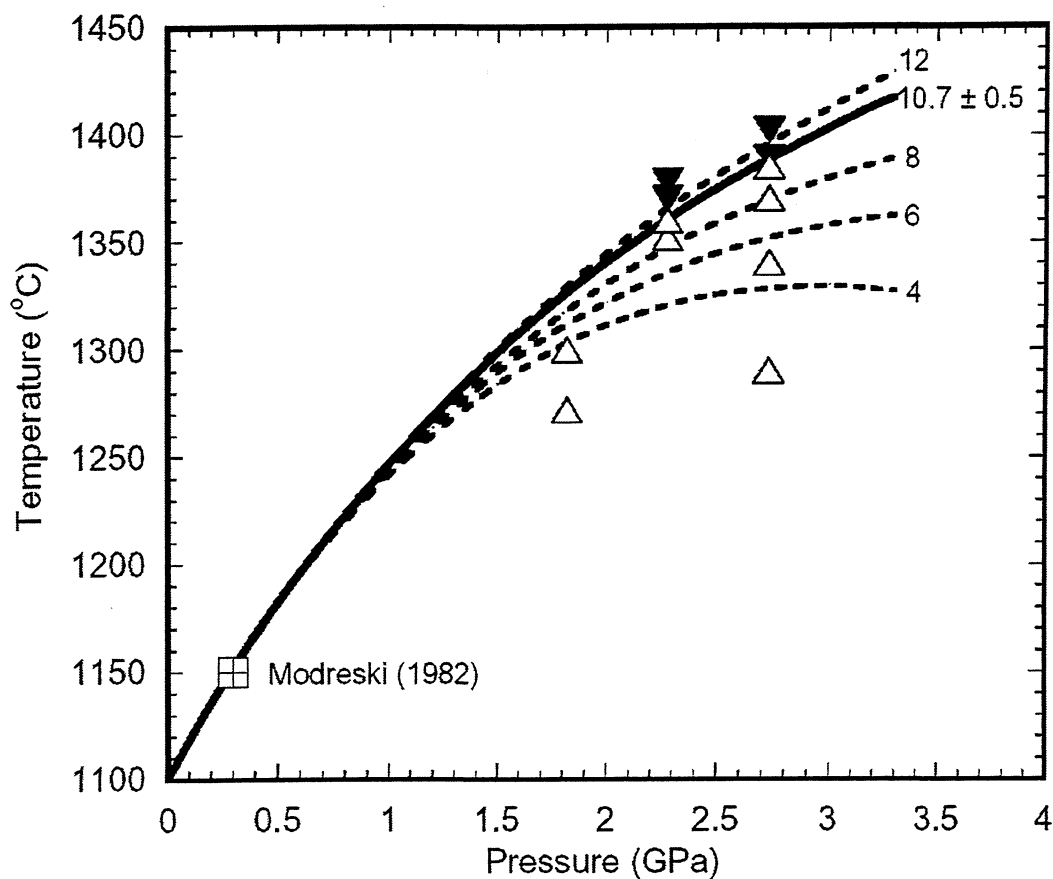
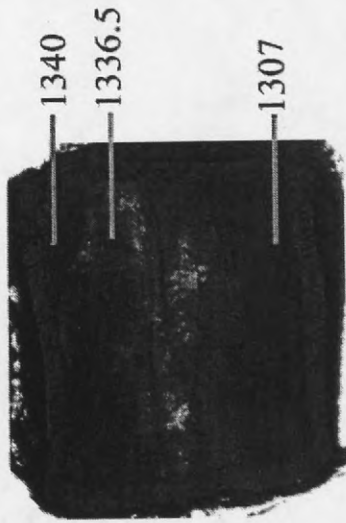
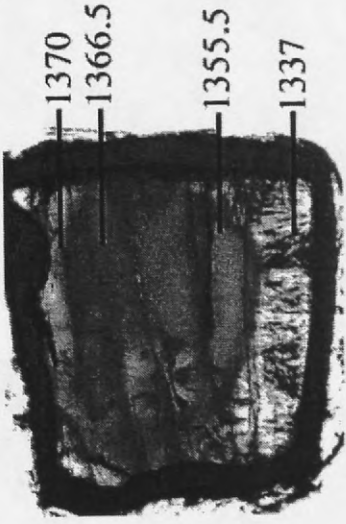


Figure 11. $\text{NaAlSi}_3\text{O}_8$ glass to crystalline experiments, along with the melting curve of albite with a K'_0 value of 10.7 ± 0.5 using the third-order Birch-Murnaghan equation of state (Birch, 1978). Dashed lines represent albite fusion curves with K'_0 values of 12, 8, 6, and 4, respectively. The phase equilibrium point of Modreski (Boettcher et al., 1982) is shown for comparison. Open triangles represent experiments in the stability field of crystalline albite, whereas closed triangles represent experiments that were in the $\text{NaAlSi}_3\text{O}_8$ liquid field. Errors in temperature and pressure are smaller than the symbols.

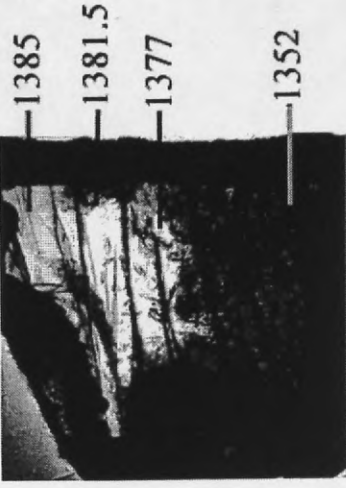
A54



A57



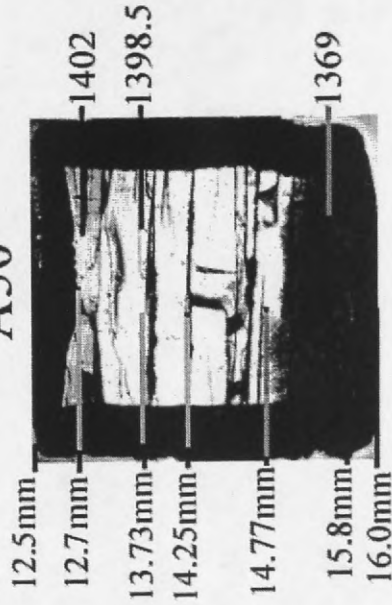
A65



A72



A50



A60

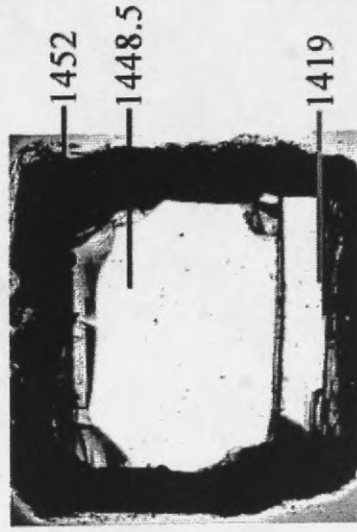


Figure 12. Plane polarized images of run products from 2.73 GPa glass to crystal experiments and the temperatures ($^{\circ}\text{C}$) based off the calculated temperature gradient in Table 2. Image A50 shows the distances from the base plug to the top of the capsule (12.5 mm), the top of the *sample* (12.7 mm), 1/3 (13.73 mm), 1/2 (14.25 mm), and 2/3 (14.77 mm) down the sample, the bottom of the sample (15.8mm), and the bottom of the capsule (16.0mm). Capsules are 3.46-3.90 mm from top to bottom.



Figure 13. Experiment A65 (1385°C) under cross-polarized light, which shows crystals, along with glass, at the top of the capsule. The Pt capsule is approximately 3.90 mm from top to bottom.

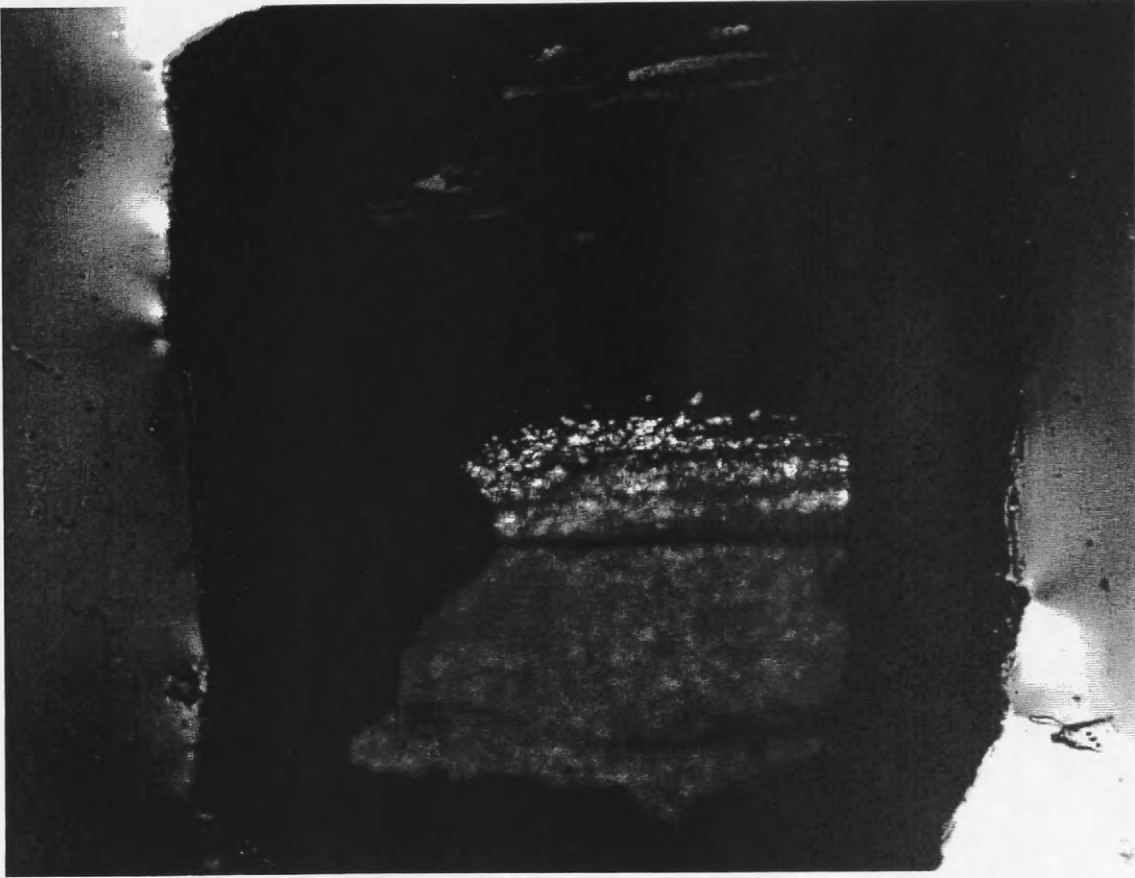


Figure 14. Experiment A72 (1389°C) under cross-polarized light, which shows the top of the capsule is entirely glass. The length is 3.71 mm from the top to the bottom of the capsule.

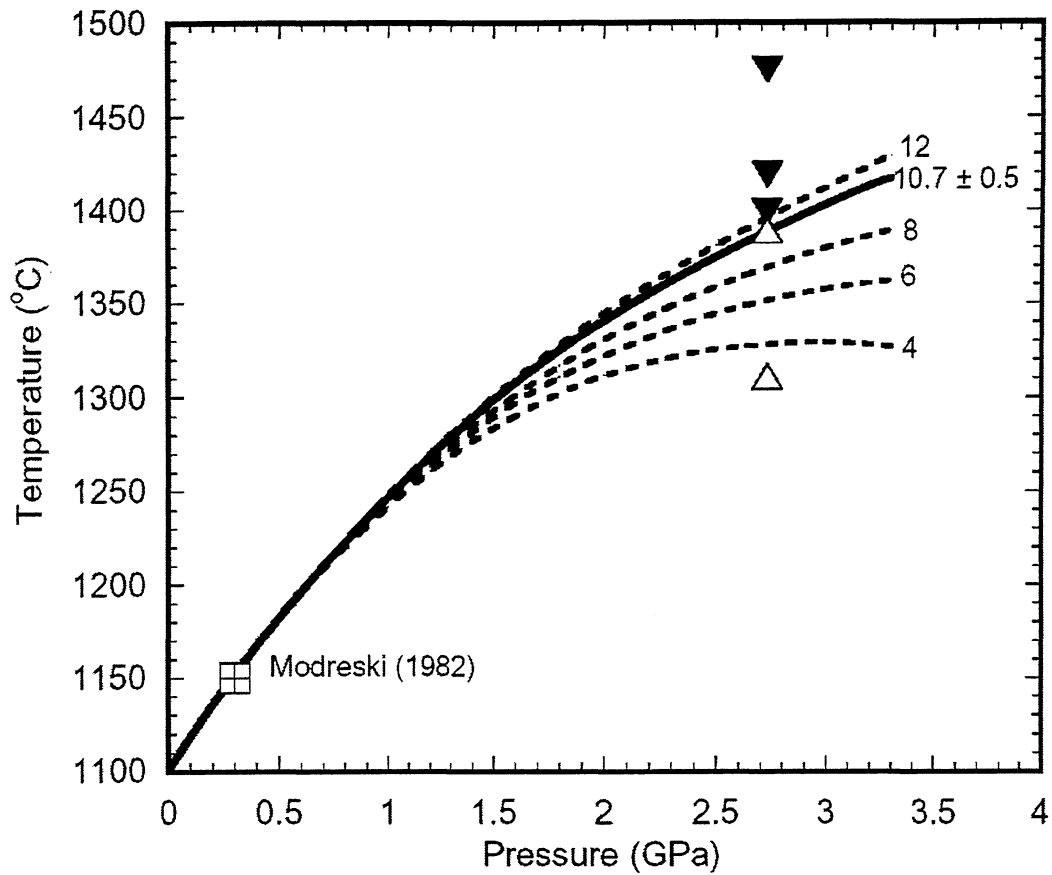


Figure 15. Crystalline high albite to glass experiments, along with the melting curve of albite with a K'_0 value of 10.7 ± 0.5 using the Birch-Murnaghan equation of state (Birch, 1978). Dashed lines represent albite fusion curves with K'_0 values of 12, 8, 6, and 4, respectively. The phase equilibrium point of Modreski is shown for comparison (Boettcher et al. 1982). Open triangles represent experiments in the crystalline albite stability field, whereas closed triangles represent experiments that were in the $\text{NaAlSi}_3\text{O}_8$ liquid field. Errors in temperature and pressure are smaller than the symbols.

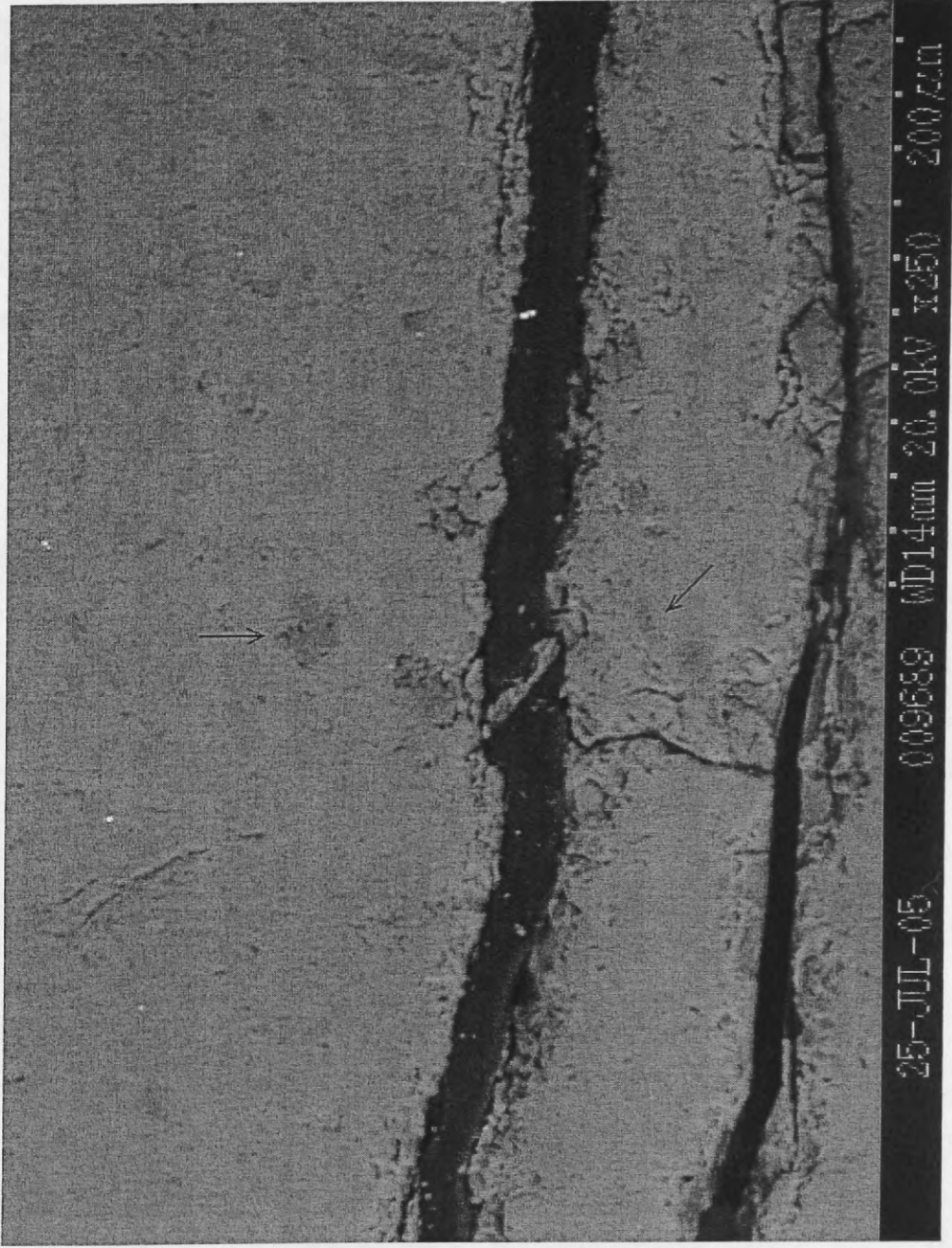


Figure 16. Backscattered electron image of the bottom (crystalline albite) of M133. Arrows indicate darker areas of MgO with the crystalline high albite. The lighter colored matrix is high albite. The small bright spots are Pt.

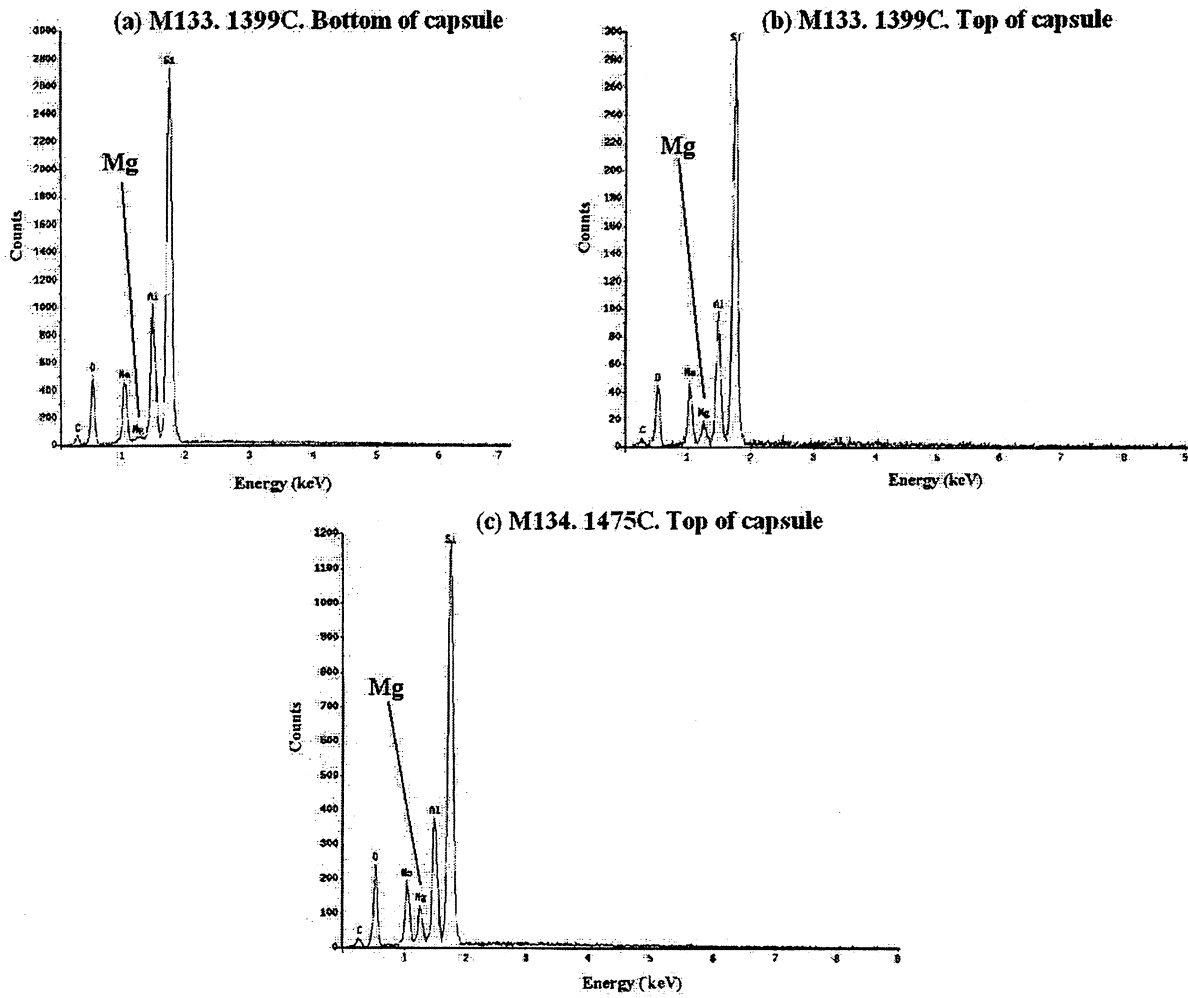


Figure 17. EDS peaks of crystalline albite (a) vs. $\text{NaAlSi}_3\text{O}_8$ glass (b and c), from run products at the University of Minnesota. Peaks b and c show that MgO is present in the liquid.

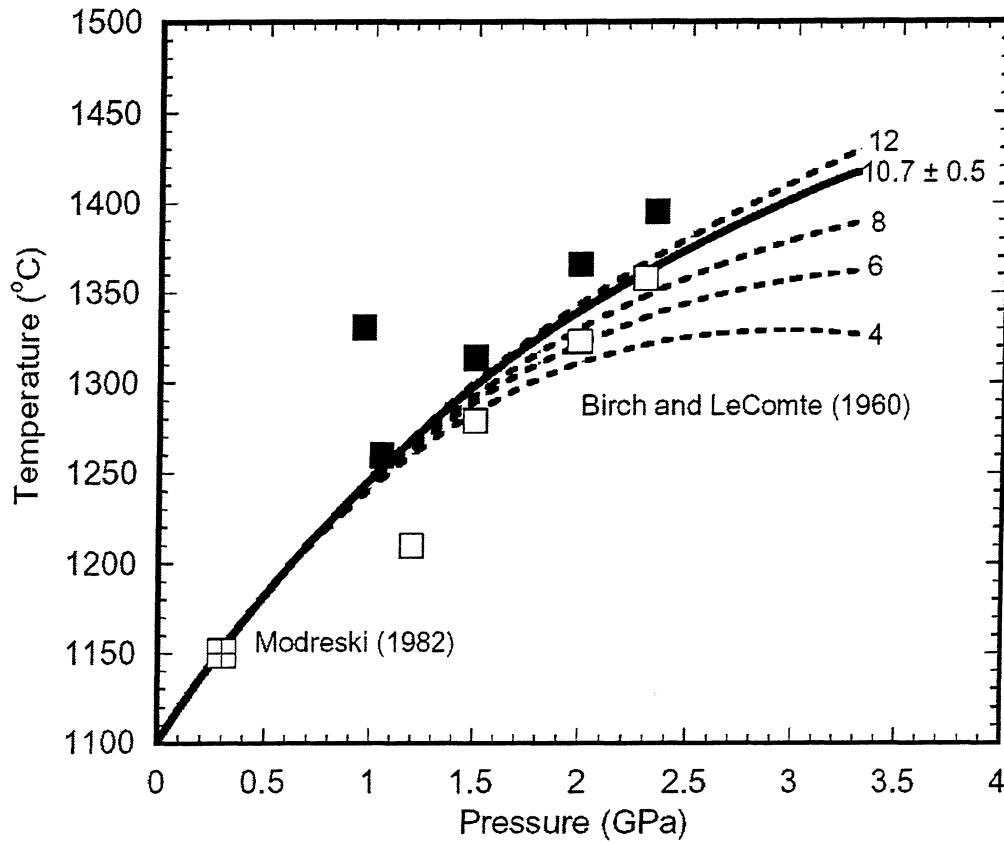


Figure 18. The experiments of Birch and LeComte (1960), along with the melting curve of albite with a K'_0 of 10.7 ± 0.5 . Dashed lines represent albite fusion curves with K'_0 values of 12, 8, 6, and 4, respectively. The phase equilibrium point of Modreski is shown for comparison (Boettcher et al. 1982). Open squares represent experiments in the crystalline albite stability field, whereas closed squares represent experiments that were in the $\text{NaAlSi}_3\text{O}_8$ liquid field. Errors in temperature and pressure are smaller than the symbols.

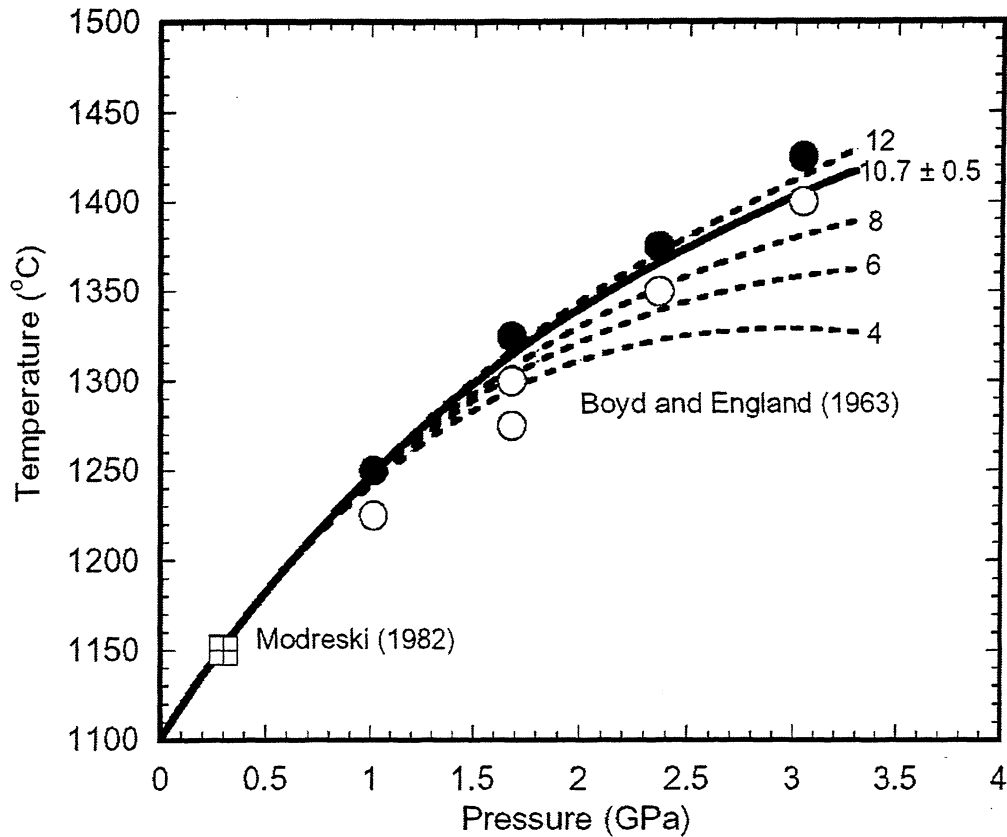


Figure 19. The pressure adjusted experiments of Boyd and England (1963), along with the melting curve of albite with a K'_0 of 10.7 ± 0.5 . Dashed lines represent albite fusion curves with K'_0 values of 12, 8, 6, and 4, respectively. The phase equilibrium point of Modreski is shown for comparison (Boettcher et al. 1982). Open circles represent experiments in the crystalline albite stability field, whereas closed circles represent experiments that were in the $\text{NaAlSi}_3\text{O}_8$ liquid field. Errors in temperature and pressure are smaller than the symbols.

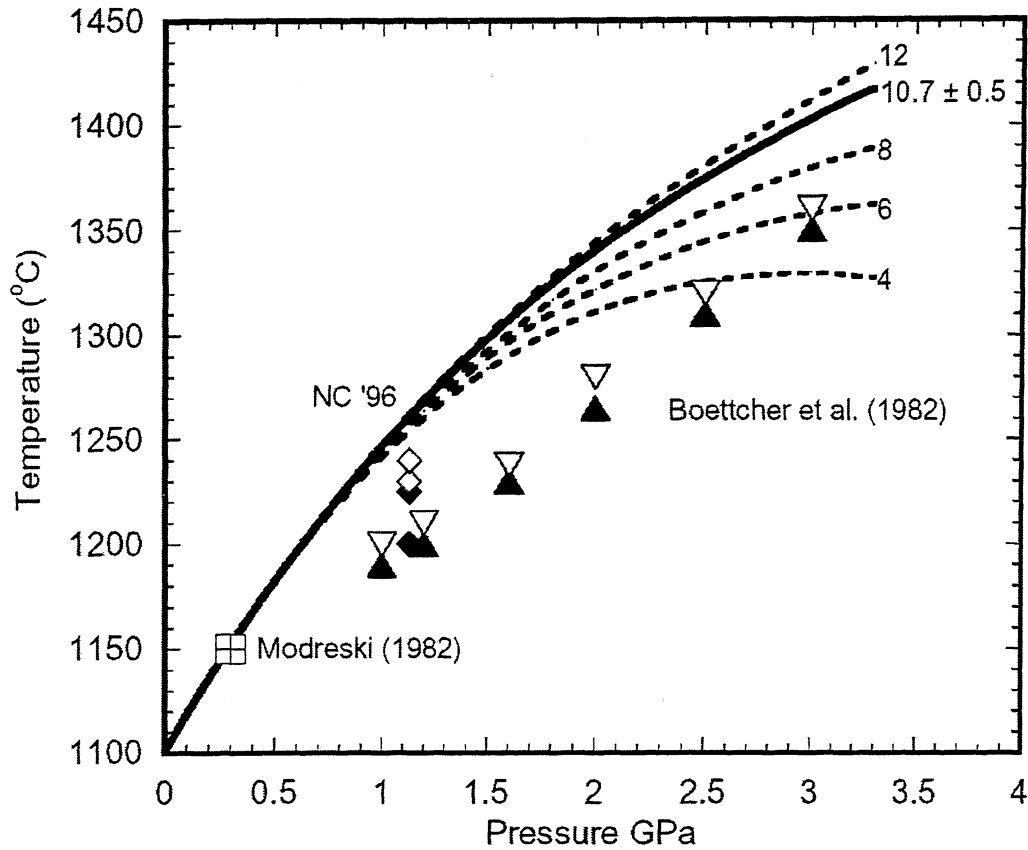


Figure 20. The experiments of Boettcher et al. (1982) (triangles) and Nekvasil and Carroll (1996) (diamonds), along with the melting curve of albite with a K'_0 of 10.7 ± 0.5 . Dashed lines represent albite fusion curves with K'_0 values of 12, 8, 6, and 4, respectively. The phase equilibrium point of Modreski is shown for comparison (Boettcher et al. 1982). Closed symbols represent experiments in the crystalline albite stability field, whereas open symbols represent experiments that were in the $\text{NaAlSi}_3\text{O}_8$ liquid field. Errors in temperature and pressure are smaller than the symbols.

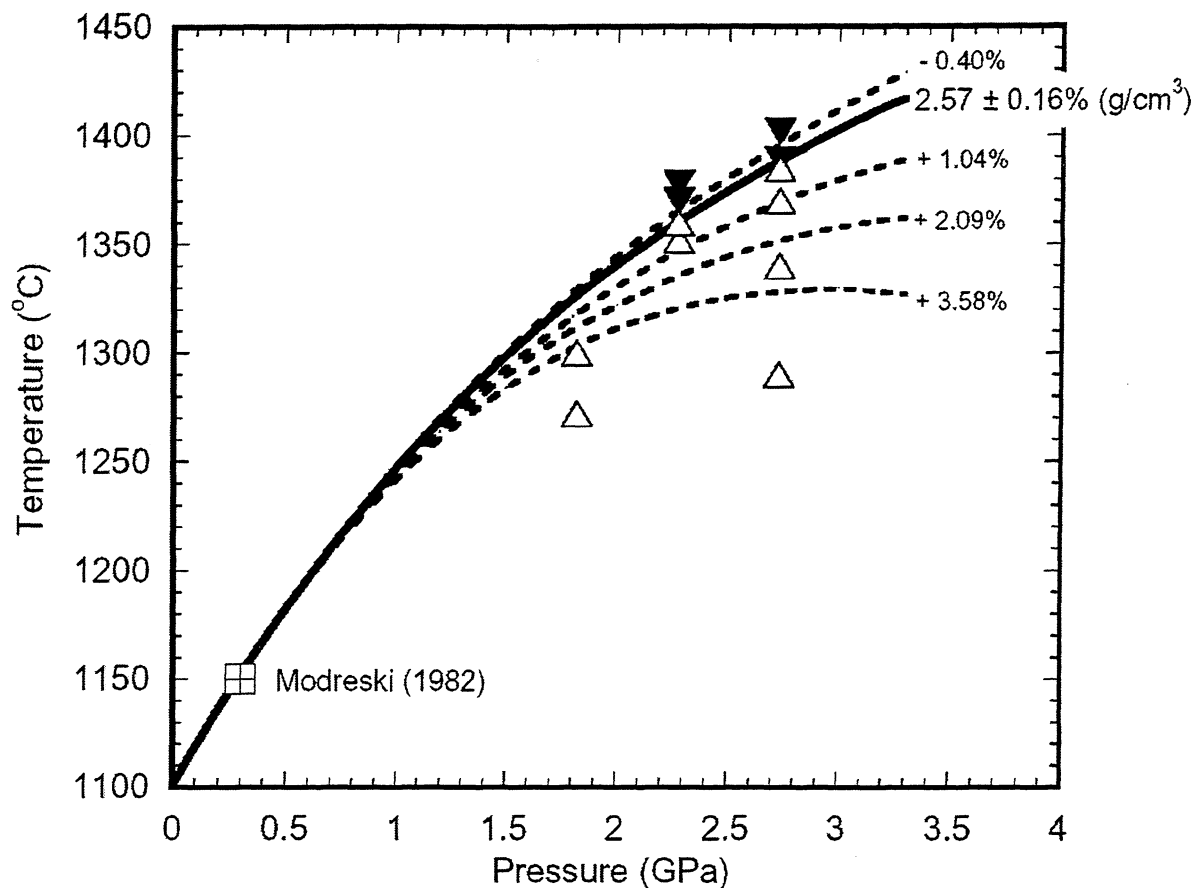


Figure 21. A plot of the various K'_0 values, and the calculated densities at 3.3 GPa and temperature. The solid line represents the density at 3.3 GPa and 1417°C ($K'=10.7 \pm 0.5$). The dashed lines represent K'_0 values of 4, 6, 8, and 12 (as in previous plots), with the difference in density reported from the temperatures (1327, 1362, 1389, and 1429°C, respectively) calculated from the thermodynamic data from Lange (2003), and the third-order Birch-Murnaghan equation of state for the respective K' values at 3.3 GPa.

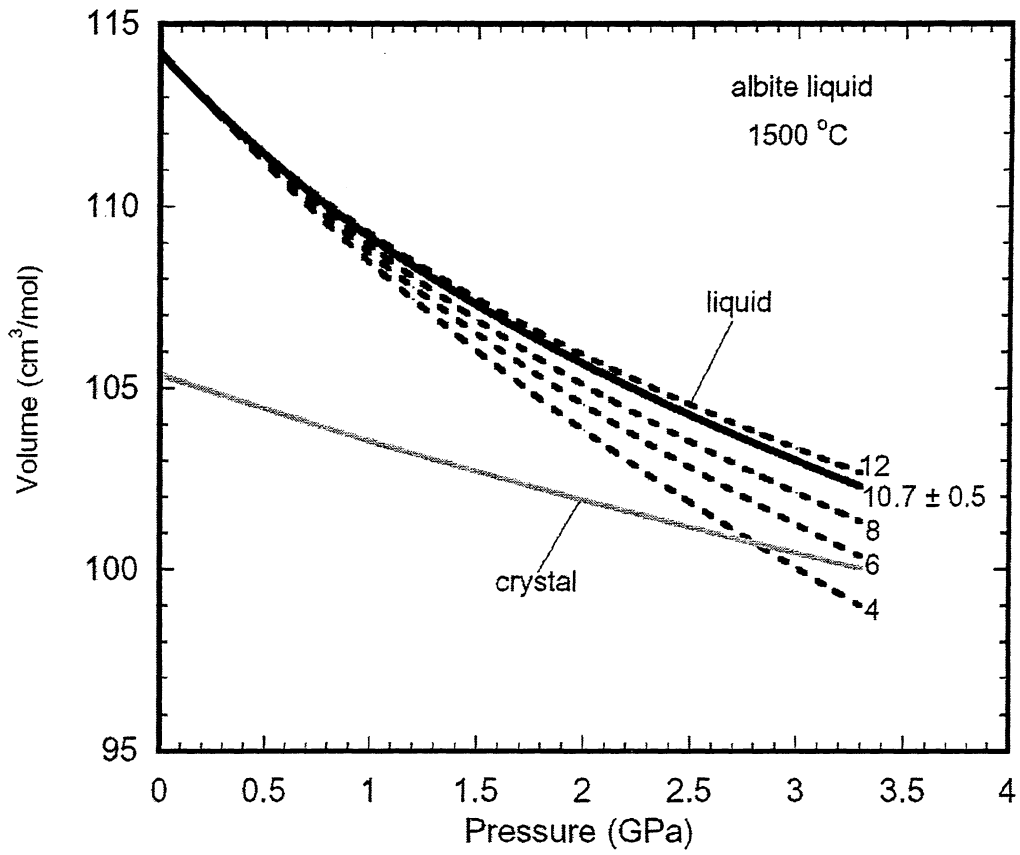


Figure 22. A comparison between the volume of liquid vs. crystalline $\text{NaAlSi}_3\text{O}_8$ as a function of pressure, using the thermodynamic data from Lange (2003) and the third-order Birch-Murnaghan equation of state. The dark solid line represents the volume of liquid $\text{NaAlSi}_3\text{O}_8$ with the K'_0 value of this study, while dotted lines represent the volume of liquid $\text{NaAlSi}_3\text{O}_8$ with K'_0 values of 12, 8, 6, and 4. The solid gray line is the volume of crystalline albite at 1500°C.

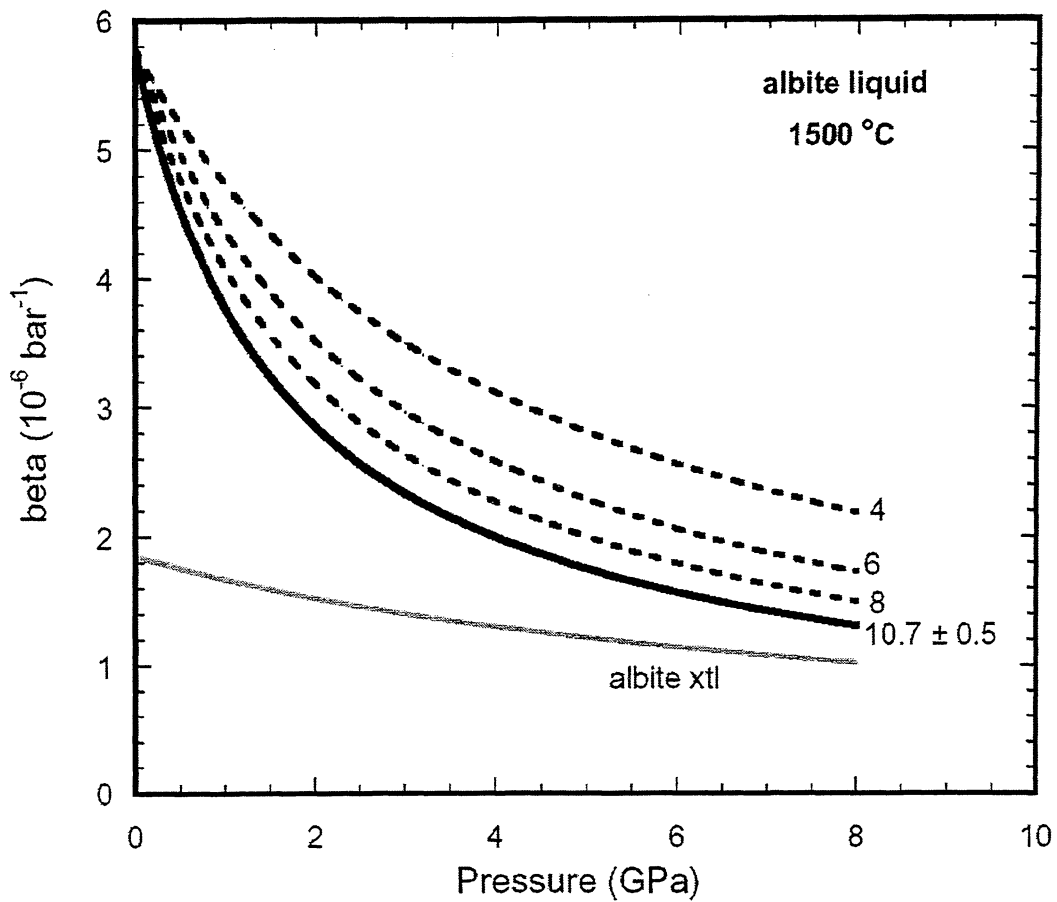


Figure 23. A plot of β_T for liquid $\text{NaAlSi}_3\text{O}_8$ as a function of pressure for various K'_0 values. For a K'_0 of 10.7, there is a pronounced curvature in the β_T function with pressure, with a substantial drop in β_T at low pressure. In contrast, lower K'_0 values decrease more steadily and less sharply over the same pressure interval.

APPENDIX

Experiment #	Distance From Base Plug (mm)	300 Data (C)	400 Data (C)	500 Data (C)	600 Data (C)	700 Data (C)	800 Data (C)
A87	7.63	274	359	442	523	605	682
A88	8.15	291	384	475	565	655	741
A84	9.8	306	406.5	506	604.5	703	800
A83	10.81	307.5	409	508.5	609	706	805.5
A82	11.87	--	--	--	--	--	--
A90	12.7	306	407	507.5	608	708	808
A82, A83, A84, A86, A87, A88, A90	14.1	300	400	500	600	700	800
A86	17.8	276	367	459	550	642	734

Experiment #	Distance From Base Plug (mm)	900 Data (C)	1000 Data (C)	1100 Data (C)	1200 Data (C)	1300 Data (C)	1391 Data (C)
A87	7.63	757	832	906	982.5	1066	1151.5
A88	8.15	827	911	995	1080	1172	1258
A84	9.8	897	992	1088	1183	1280	1369
A83	10.81	903.5	1002	1099	1196	1295	1387
A82	--	--	--	--	--	--	1393
A90	12.7	909	1009	1108.5	1208	1307	1398.5
A82, A83, A84, A86, A87, A88, A90	14.1	900	1000	1100	1200	1300	1391
A86	17.8	826	919	1013	1110	1211	1304.5

Figure 1. Data collected at each 100 degree interval for all experiments.

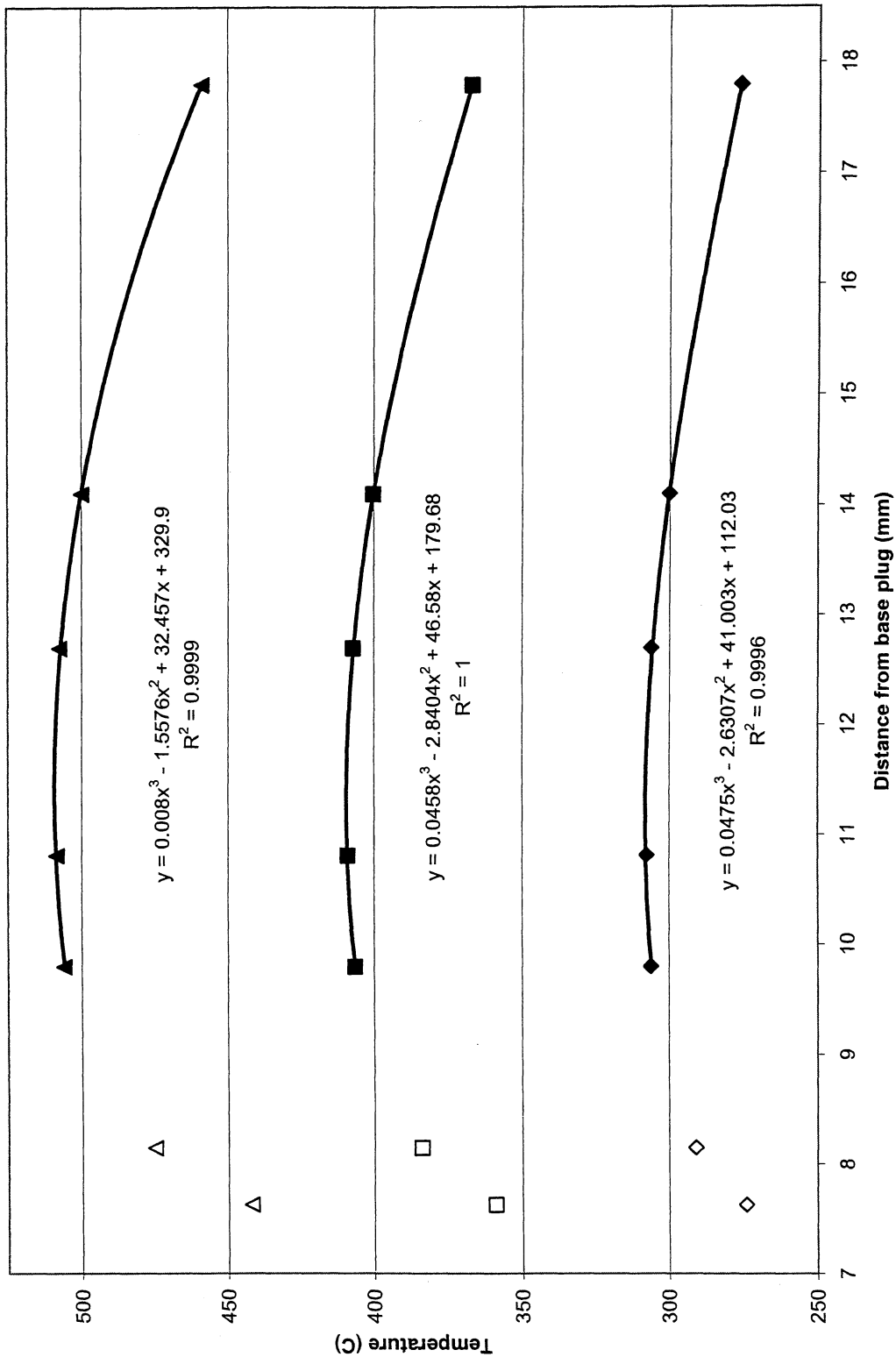


Figure 2. Graphical plots of 300-500°C data, along with the polynomial best fit.

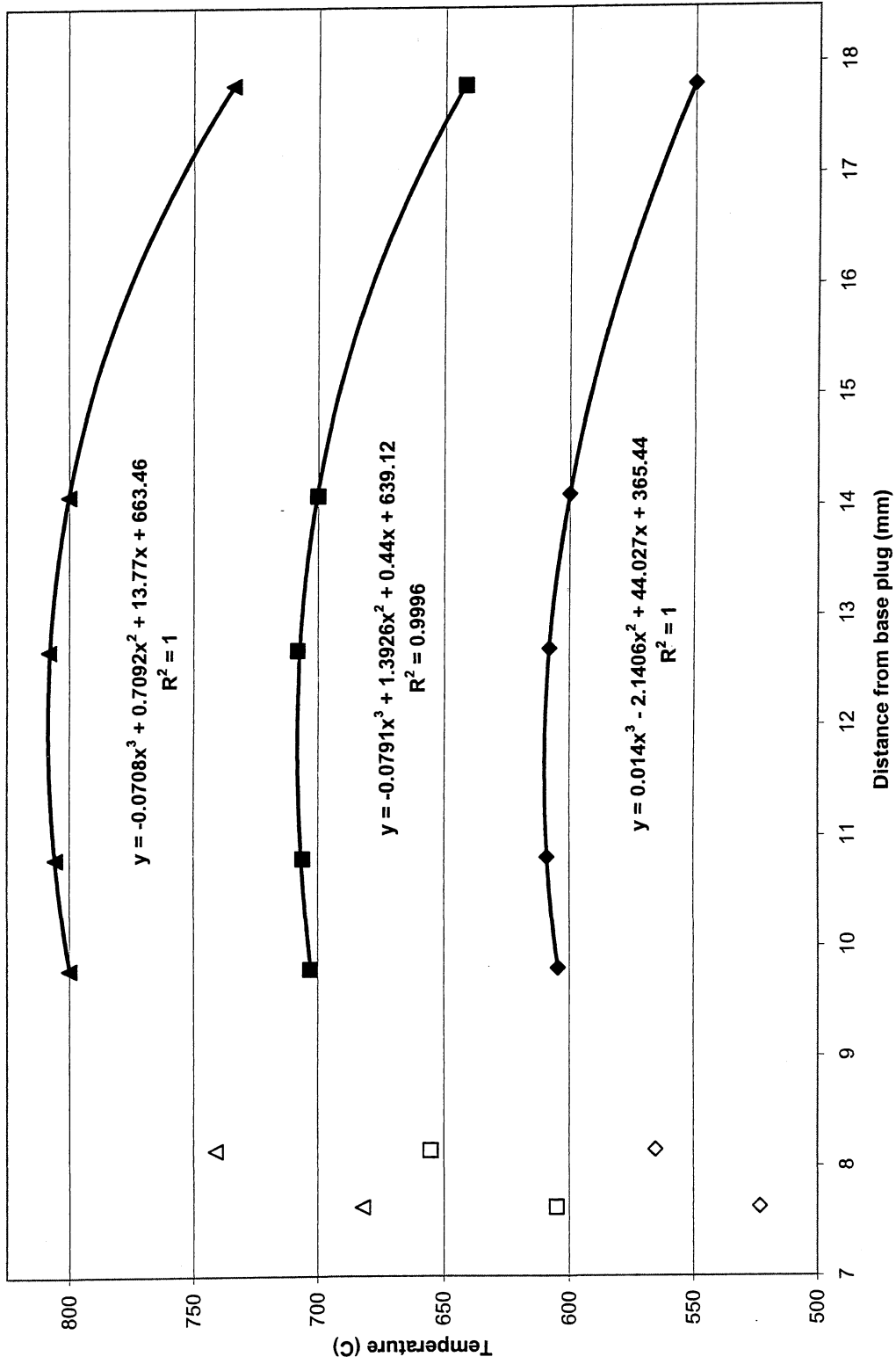


Figure 3. Graphical plots of 600-800°C data, along with the polynomial best fit.

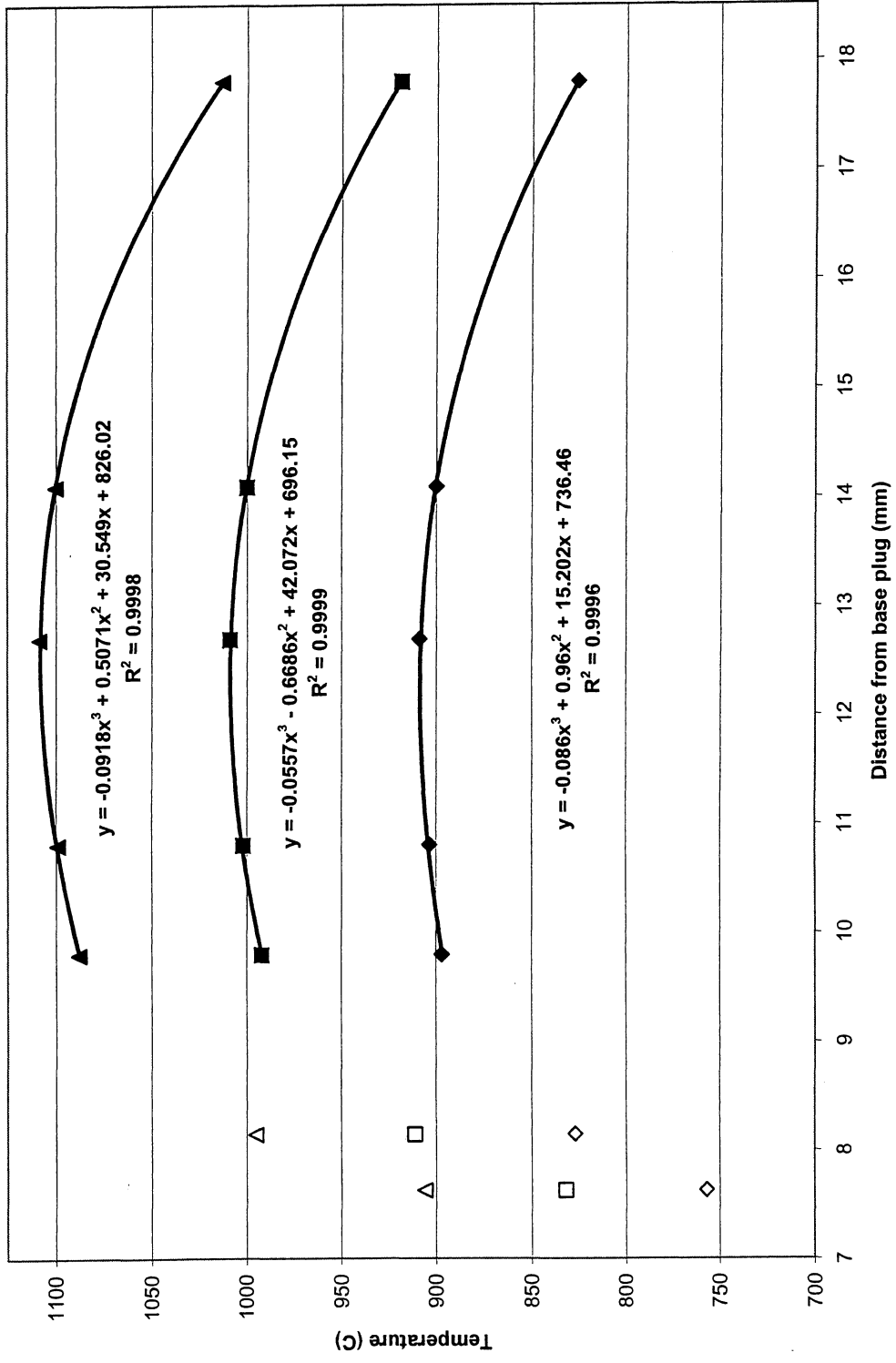


Figure 4. Graphical plots of 900-1100°C data, along with the polynomial best fit.

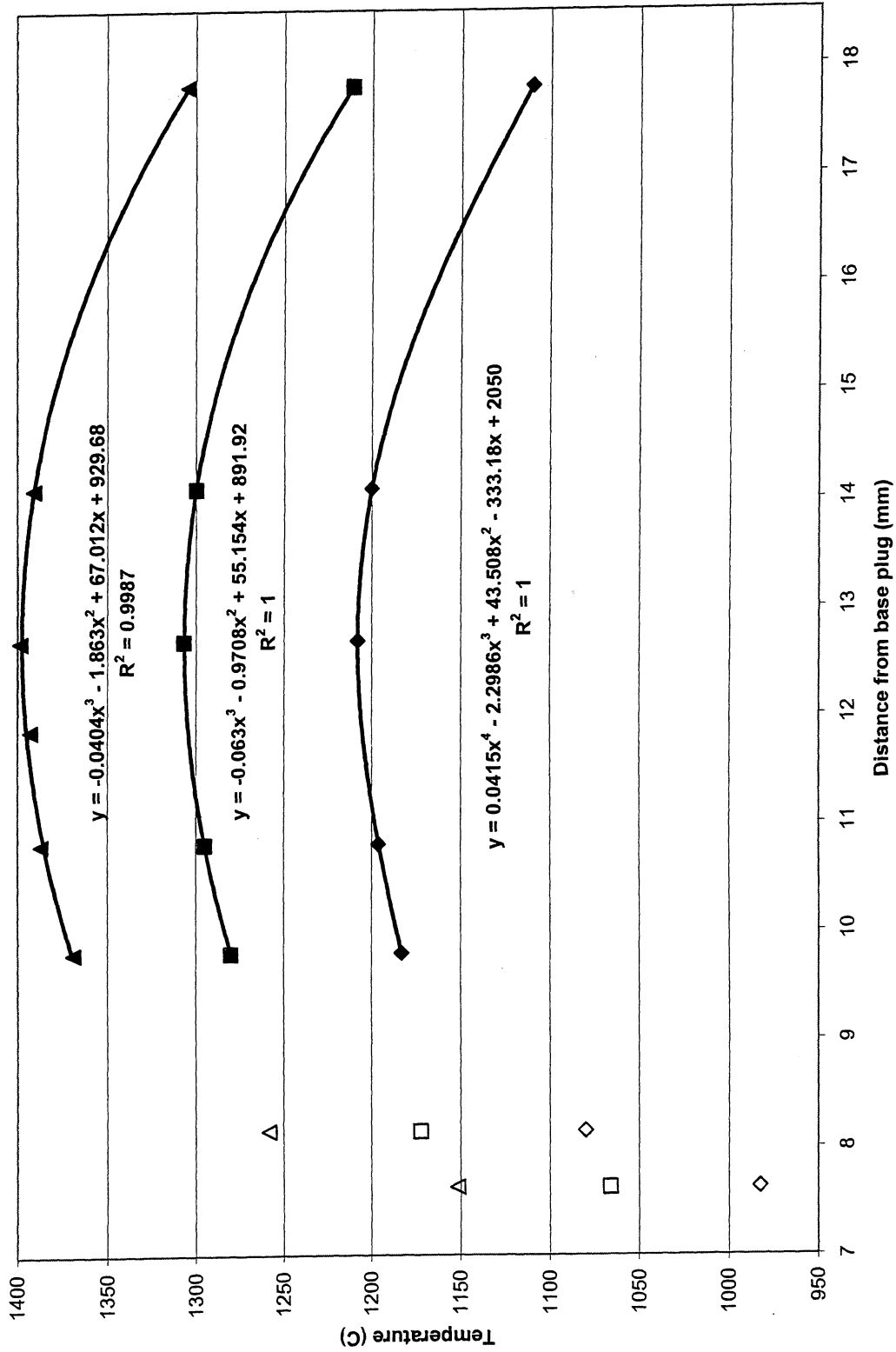


Figure 5. Graphical plots of 1200-1391°C data, along with the polynomial best fit.

From 300 Data			From 400 Data			From 500 Data		
Temp °C	Distance From Base Plug, mm	Temp °C	Distance From Base Plug, mm	Temp °C	Distance From Base Plug, mm	Temp °C	Distance From Base Plug, mm	Temp °C
308.0	11.15	409.4	11.2	509.3	11.35	509.3	11.35	509.3
308.0	11.2	409.4	11.25	509.3	11.4	509.3	11.4	509.3
308.0	11.25	409.4	11.3	509.3	11.45	509.3	11.45	509.3
307.3	12	408.8	12	508.9	12	508.9	12	508.9
306.3	12.5	407.6	12.5	507.9	12.5	507.9	12.5	507.9
305.8	12.7	406.9	12.7	507.3	12.7	507.3	12.7	507.3
302.0	13.73	402.3	13.73	502.6	13.73	502.6	13.73	502.6
299.6	14.25	399.2	14.25	499.3	14.25	499.3	14.25	499.3
296.8	14.77	395.6	14.77	495.3	14.77	495.3	14.77	495.3
290.5	15.8	387.2	15.8	485.4	15.8	485.4	15.8	485.4
289.2	16	385.4	16	483.2	16	483.2	16	483.2

From 600 Data			From 700 Data			From 800 Data		
Temp °C	Distance From Base Plug, mm	Temp °C	Distance From Base Plug, mm	Temp °C	Distance From Base Plug, mm	Temp °C	Distance From Base Plug, mm	Temp °C
610.0	11.55	708.3	11.85	808.5	12	808.5	12	808.5
610.0	11.6	708.3	11.9	808.5	12.05	808.5	12.05	808.5
610.0	11.65	708.3	11.95	808.5	12.1	808.5	12.1	808.5
609.7	12	708.2	12	808.1	12.5	808.1	12.5	808.1
608.7	12.5	707.7	12.5	807.7	12.7	807.7	12.7	807.7
608.0	12.7	707.3	12.7	803.0	13.73	803.0	13.73	803.0
602.6	13.73	703.0	13.73	798.8	14.25	798.8	14.25	798.8
598.7	14.25	699.3	14.25	793.4	14.25	793.4	14.25	793.4
593.9	14.77	694.5	14.77	778.8	14.77	778.8	14.77	778.8
581.9	15.8	681.7	15.8	775.3	15.8	775.3	15.8	775.3
579.2	16	678.7	16	775.3	16	775.3	16	775.3

Figure 3. Hotspot location (in bold) and thermal gradients as calculated by the polynomial best fit curves of the data from 300-800°C. The shift in the hotspot upward from the center of the 30 mm furnace is consistent with the findings of Pickering et al. (1998).

From 900 Data		From 1000 Data		From 1100 Data	
Temp °C	Distance From Base Plug, mm	Temp °C	Distance From Base Plug, mm	Temp °C	Distance From Base Plug, mm
908.5	12	1008.5	12	1107.0	12
908.6	12.2	1008.8	12.3	1107.8	12.5
908.7	12.25	1008.8	12.35	1107.8	12.55
908.6	12.3	1008.8	12.4	1107.8	12.6
908.5	12.5	1008.8	12.5	1107.7	12.7
908.2	12.7	1008.5	12.7	1103.4	13.73
903.6	13.73	1003.6	13.73	1098.7	14.25
899.2	14.25	998.7	14.25	1092.1	14.77
893.3	14.77	992.2	14.77	1073.2	15.8
877.1	15.8	974.3	15.8	1068.6	16
873.2	16	970.0	16		

From 1200 Data		From 1300 Data		From 1391 Data	
Temp °C	Distance From Base Plug, mm	Temp °C	Distance From Base Plug, mm	Temp °C	Distance From Base Plug, mm
1205.8	12	1305.1	12	1395.7	12
1207.1	12.5	1306.6	12.5	1397.3	12.5
1207.2	12.6	1306.7	12.65	1397.5	12.65
1207.2	12.65	1306.7	12.7	1397.5	12.7
1207.2	12.7	1306.7	12.75	1397.5	12.75
1203.5	13.73	1303.1	13.73	1394.0	13.73
1198.8	14.25	1298.4	14.25	1389.4	14.25
1192.1	14.77	1291.8	14.77	1382.9	14.77
1172.7	15.8	1272.5	15.8	1364.0	15.8
1168.0	16	1267.8	16	1359.5	16

Figure 3. Hotspot location (in bold) and thermal gradients as calculated by the polynomial best fit curves of the data from 900-1391°C. The shift in the hotspot upward from the center of the 30 mm furnace is consistent with the findings of Pickering et al. (1998).

UNIVERSITY OF MICHIGAN



3 9015 06998 2018